

## PLANETESIMAL CLEARING AND SIZE-DEPENDENT ASTEROID RETENTION BY SECULAR RESONANCE SWEEPING DURING THE DEPLETION OF THE SOLAR NEBULA

XIAOCHEN ZHENG(郑晓晨)<sup>1,2,3,4,8</sup>, DOUGLAS N.C. LIN(林潮)<sup>2,3,5,6,9</sup>, AND M.B.N. KOUWENHOVEN(柯文采)<sup>7,2,10</sup><sup>1</sup>Department of Astronomy, Peking University, Yiheyuanlu 5, Haidian District, Beijing 100871, P.R. China<sup>2</sup>Kavli Institute for Astronomy and Astrophysics, Peking University, Yiheyuanlu 5, Haidian District, Beijing 100871, P.R. China<sup>3</sup>Department of Astronomy and Astrophysics, University of California, Santa Cruz, CA 95064, USA<sup>4</sup>Center for Astrophysics, Tsinghua University, Shuangqing Rd. 30, Haidian District, Beijing 100084, China<sup>5</sup>Institute for Advanced Studies, Tsinghua University, Shuangqing Rd. 30, Haidian District, Beijing 100084, China<sup>6</sup>National Astronomical Observatory of China, Datun Rd., Chaoyang District, Beijing 100012, P.R. China<sup>7</sup>Department of Mathematical Sciences, Xi'an Jiaotong-Liverpool University, 111 Ren'ai Rd., Suzhou Dushu Lake Science and Education Innovation District, Suzhou Industrial Park, Suzhou 215123, P.R. China<sup>8</sup>x.c.zheng1989@gmail.com<sup>9</sup>lin@ucolick.org<sup>10</sup>t.kouwenhoven@xjtlu.edu.cn

## ABSTRACT

The distribution of heavy elements is anomalously low in the asteroid main belt region compared with elsewhere in the solar system. Observational surveys also indicate a deficit in the number of small ( $\lesssim 50$  km size) asteroids that is two orders of magnitude lower than what is expected from the single power-law distribution that results from a collisional coagulation and fragmentation equilibrium. Here, we consider the possibility that a major fraction of the original asteroid population may have been cleared out by Jupiter's secular resonance, as it swept through the main asteroid belt during the depletion of the solar nebula. This effect leads to the excitation of the asteroids' orbital eccentricities. Concurrently, hydrodynamic drag and planet-disk tidal interaction effectively damp the eccentricities of sub-100 km-size and of super-lunar-size planetesimals, respectively. These combined effects lead to the asteroids' orbital decay and clearing from the present-day main belt region ( $\sim 2.1 - 3.3$  AU). Eccentricity damping for the intermediate-size (50 to several hundreds of kilometers) planetesimals is less efficient than for small or large planetesimals. These objects therefore preferentially remain as main belt asteroids near their birthplaces, with modest asymptotic eccentricities. The smaller asteroids are the fragments of subsequent disruptive collisions at later times as suggested by the present-day asteroid families. This scenario provides a natural explanation for both the observed low surface density and the size distribution of asteroids in the main belt, without the need to invoke special planetesimal formation mechanisms. It also offers an explanation for the confined spatial extent of the terrestrial planet building blocks without the requirement of extensive migration of Jupiter, which is required in the grand-tack scenario.

*Keywords:* minor planets, asteroids: general – planetary systems – planet-disc interactions – methods: numerical – planets and satellites: dynamical evolution and stability – protoplanetary discs

## 1. INTRODUCTION

The formation and evolution of planetesimals are essential steps in the classical core accretion model for the origin of planets (Pollack et al. 1996; Ida & Lin 2004). The conventional coagulation scenario (Safronov 1969; Wetherill 1980) is based on the assumption that these planetary building blocks grow due to cohesive collisions through a runaway process, followed by an oligarchic phase (Kokubo & Ida 1998). The crater-covered surfaces of asteroids, the Moon, and Mercury provide vivid supporting evidence for such an assumption. These collisions are generally preceded by close elastic encounters that excite the planetesimals' eccentricities and induce orbit crossing.

Through scattering and collisions, planetesimals attain an equilibrium velocity dispersion,  $\sigma$ . In a gas-free environment, the magnitude of  $\sigma$  is a significant fraction of their characteristic surface escape speeds (Aarseth 1993; Palmer et al. 1993; Kokubo & Ida 1998). At such a high speed, many collisions among super-kilometer-size planetesimals may lead to breakup rather than a merger (Agnor & Asphaug 2004; Leinhardt & Stewart 2012; Stewart & Leinhardt 2012). Direct evidence of collisional fragmentation can be found in iron/stone meteorites. Their parent bodies were differentiated prior to catastrophic collisions. The much more common chondritic meteorites may

also be the collisional by-products of parent bodies that may have avoided differentiation because they formed after the radioactive  $^{26}\text{Al}$  isotopes have mostly decayed.

The possibility of collisional fragmentation poses a potential barrier for planetesimal formation and growth. In attempts to explore pathways to bypass the kilometer-size coagulation barrier, several scenarios have been proposed. Grains and planetary building block materials may be trapped in regions with a local pressure maximum, where the flow is Keplerian and the planetesimals'  $\sigma$  is relatively small, to promote cohesive rather than disruptive collisions. One such a location is the snow line (Kretke & Lin 2007; Brauer et al. 2008) which, during the advanced stages of solar nebula evolution, may have been located close to or interior to the present-day asteroid belt (Garaud & Lin 2007). Other growth hypotheses that have been proposed and analyzed so far include gravitational instability (Goldreich & Ward 1973; Weidenschilling & Cuzzi 1993; Youdin & Shu 2002; Garaud & Lin 2004), streaming instability (Youdin & Goodman 2005), and turbulent trapping (Cuzzi 1993; Johansen et al. 2007).

While most planetesimals may eventually be accreted by a few massive embryos to form either terrestrial planets or progenitor cores of gas giants (Ida & Lin 2004), some relics are retained in the asteroid belt. The dynamics, structure, and composition of the asteroids carry important information on the chronology and dominant physical processes associated with planetesimal and planet formation. One particularly important clue is the asteroids' size-frequency distribution (SFD). Conventional coagulation models predict a power-law spectrum (Dohnanyi 1969) that generally matches that of impactors thought to have produced the observed crater size distributions on the Moon and on Mercury. In contrast, the alternative collective mechanisms lead to a rapid emergence of preferentially large planetesimals.

The observed SFD in the present-day main belt ( $\sim 2.1 - 3.3$  AU) is dominated by the midsize asteroids, with an apparent lack of small (sub-kilometer-size) and large (moon-size) bodies (Bottke et al. 2005). Based on the assumption that planetesimals formed through collective mechanisms (Johansen et al. 2007; Cuzzi et al. 2008) with a minimal size around 100 km, Morbidelli et al. (2009) reproduced the observed SFD slope. However, the rapid formation of relatively large planetesimals also implies that they are likely to have acquired similar quantities of radioactive  $^{26}\text{Al}$  isotopes, as those found in the most primitive Calcium-Aluminium-rich inclusions (CAIs). Under such conditions, the heat released from nuclear fission would be adequate to melt and differentiate planetesimals with sizes larger than a few tens of kilometers (McSween 1999). Under the rapid formation scenario, first-generation large planetesimals are likely to be differentiated. Cosmochemical analysis of iron meteorites (Kelley & Gaffey 2000) suggests that there may indeed have been 50 – 100 differentiated parent bodies that acquired their relatively large mass at sufficiently early time. However, the undifferentiated chondritic meteorites make up the predominant population of meteorites that struck the Earth. Since most meteorites originate from the asteroid belt, if a population of large planetesimals did emerge very early (within a few hundred thousand years), they and their collisional fragments would have to be preferentially cleared out of the main belt region.

The empirical *minimum mass solar nebula* (MMSN) model (Hayashi 1981; Weidenschilling et al. 1997) and the conventional formation model for large asteroids and chondritic meteorites in the main belt are constructed based on the assumption that the mass distribution (in both gas and refractory solids) is continuous throughout the solar nebula (Wetherill 1989; Connolly et al. 1998; Ciesla & Hood 2002; Desch & Connolly 2002; Johansen et al. 2007). However, the total present-day mass of the asteroids, estimated from Mars's orbit and the asteroids' observed SFD, is  $\sim 6 \times 10^{-4}$  Earth masses (Morbidelli et al. 2009). This apparent depression in the mass distribution, relative to the MMSN model, suggests that up to 99.9% of the residual planetesimals' total mass may have been lost from the main belt region. In the context of the “grand-tack” model, Walsh et al. (2011) put forward the possibility of inward-then-outward migration of Jupiter and Saturn, which may have migrated to the present-day location of the main belt prior to the disk depletion. As a consequence, asteroids in the main belt are severely depleted and repopulated during the phase of the gas giants' instability.

In this work we propose an alternative scenario to account for the observed SFD and the mass deficit in the main asteroid belt, based on the classical planetesimal coagulation (rather than the collective formation) model. We assume that coagulation and fragmentation of asteroids occurred within 2 Myr (which is comparable to the radiogenic age of the chondritic meteorites) when the energy release rate from the decay of  $^{26}\text{Al}$  has largely diminished. We also assume that these processes lead to a continuous SFD ranging from dust to lunar-size protoplanetary embryos (Chambers 2008) with a total mass several times that of the Earth.

In order to reproduce the observed SFD and the present-day low surface density in the main belt region, we propose that the small and large planetesimals were cleared by  $\nu_{5,6}$  secular resonance (SR) that swept through the region during the local clearing and global depletion of the solar nebula (e.g. Heppenheimer 1980; Ward 1981; Lemaître & Dubru 1991; Lecar & Franklin 1997; Nagasawa & Ida 2000; Nagasawa et al. 2000, 2001, 2002; O'Brien et al. 2007, and references therein). We suggest that this process occurred after the formation of Jupiter and on a time scale of  $\sim 3 - 5$  Myr, comparable to the observed depletion time scale of protostellar disks (Hartmann 1998) and the radiogenic age difference between the CAIs and chondrules.

The sweeping secular resonances (SSRs) excite the eccentricities of all planetesimals along their path. The eccentricities of the small (sub-kilometer-size) rocky bodies and large (Moon-size) embryos are effectively damped by the

hydrodynamic drag and planet-disk tidal interaction. Consequently, these planetesimals undergo orbital decay synchronously with the inward sweeping of the  $\nu_5$  SR (Nagasawa et al. 2005; Thommes et al. 2008). As an extension of these previous investigations, we show that some intermediate-size planetesimals are retained in the main belt because their eccentricity damping and orbital decay are less effective.

This paper is structured as follows. In §2, we briefly recapitulate the basic physical effects of the sweeping SRs, and we describe our numerical method and initial conditions in §3. In §4 we compute the orbital evolution for planetesimals with a range of sizes. Based on these results, we reconstruct the asteroids’ SFD and the mass depletion rate of the asteroid belt under the combined effects of SSRs and eccentricity damping. We compare our results with observations and discuss the implications in §5.

## 2. BRIEF DESCRIPTION OF THE SSRS

We briefly recapitulate the physical concept of the dynamical shake-up model, which was proposed in the context of terrestrial planet formation by Nagasawa et al. (2005) and Thommes et al. (2008). This model is based on the following assumptions that (i) the initial growth of planetesimals of an unperturbed gaseous solar nebula was limited by their isolation mass  $M_{\text{iso}}$ . In an MMSN,  $M_{\text{iso}} < M_{\oplus}$  within a few astronomical units, but beyond the snow line embryos may acquire super-Earth masses (Ida & Lin 2004). (ii) Relatively massive ( $> 10 M_{\oplus}$ ) embryos can efficiently accrete gas (Pollack et al. 1996) and evolve into Jupiter and Saturn within  $\sim 2$  Myr. (iii) Gas in the solar nebula was depleted over a characteristic time scale ( $\sim 3 - 5$  Myr), comparable to that observed in disks around T Tauri stars (Hartmann 1998).

In addition, we assume that gravitational interaction between the emerging gas giants and nearby embryos and planetesimals induced scattering and giant impacts during their formation (Li et al. 2010; Ida et al. 2013). These close encounters lead not only to orbit crossing (Zhou et al. 2007) and compositional mixing of residual planetesimals (DeMeo & Carry 2014), but also to eccentricity excitation of the emerging planets. With a finite eccentricity, Jupiter and Saturn exert a secular perturbation on the residual planetesimals, causing their eccentricities to modulate and their longitudes of periastron to precess (Murray & Dermott 1999). This perturbation is particularly strong near the gas giants’ low-order mean motion resonances (MMRs). Due to the self-gravity of the nebula, Jupiter’s and Saturn’s orbits also precess. In regions where two precession frequencies match, the SRs excite the planetesimals’ eccentricities as angular momentum is monotonically transferred from the planetesimals to the gas giants.

In principle, all the planets contribute to the secular perturbation. Two particularly strong SRs among these are the  $\nu_5$  and  $\nu_6$  SRs. They are dominated by the perturbations from Jupiter and Saturn, respectively (Agnor & Lin 2012). In this paper, we include these additional planetary contributions. However, contribution to the gas giants’ precession rates by the disk potential is comparable to that induced by Jupiter’s and Saturn’s interactions. When the solar nebula’s mass distribution was comparable to that of the MMSN model, the  $\nu_5$  SR was located near the asteroids’ main belt. During the advanced stages of nebula evolution, the precession rates induced by the disk decline with its diminishing surface density ( $\Sigma$ ), resulting in the locations of these resonances sweeping through the solar system. Today, the nebula is completely cleared of gas and the  $\nu_5$  SR is located interior to the orbit of Venus, whereas the  $\nu_6$  SR is beside the terrestrial planet region, between the previous orbit of Mars and the main asteroid belt.

## 3. COMPUTATIONAL MODELS

Our work mainly focuses on the combined effects of two competitive processes: eccentricity excitation by MMRs and SRs and eccentricity damping of the progenitors of the modern-day asteroids during the advanced stages of solar nebula evolution (a few Myr after CAI formation). In this section we show that both small planetesimals and large embryos are preferentially cleared out from the main asteroid belt region, and discuss how these processes result in the observed SFD of the present-day asteroid belt.

### 3.1. Numerical method

In this paper we propose that orbital decay associated with the sweeping SR is the main cause of size-selected clearing of the asteroid population from the main belt region. In order to quantitatively establish this conjecture, we present the results of a series of numerical simulations. The computational tool we employ is a modified version of the publicly available HERMIT4 package (Aarseth 2003), which is ideally suited to carry out planetary system simulations.

We consider systems consisting of the Sun, Jupiter, and Saturn. For most models, including the default model, the two gas giant planets are initialized at their present-day locations, with eccentricities slightly different from their present-day values. The planetesimals are represented by a population of coplanar (with respect to the giant planet) particles with initial semimajor axes distributed in the current domain of the main asteroid belt. These particles can be treated as massless, such that we can neglect their gravitational perturbation on the disk and on the gas giants, as well as their mutual gravitational interactions.

The internal density of asteroids inferred from their orbital dynamics is in the range  $1 - 5 \text{ g/cm}^3$  (Margot et al. 2002; Marchis et al. 2006; Descamps & Marchis 2008). We assume that differentiation and fragmentation may have

occurred among relatively large planetesimals, whereas small planetesimals may be considered to be pristine rubble piles. We construct a simple prescription for the planetesimals' internal density, ranging from that of iron/stone meteorites with zero porosity ( $\rho_p = 5.5 \text{ g/cm}^3$ ) for the relatively large (with radius  $r_p > 100 \text{ km}$ ) planetesimals to that of water ice ( $\rho_p = 1 \text{ g/cm}^3$ ) for the small planetesimals ( $r_p < 18 \text{ km}$ ). We also assume a transitional density  $\rho_p(r_p) = (r_p/18 \text{ km}) \text{ g/cm}^3$  for the intermediate-size ( $18 \text{ km} \leq r_p \leq 100 \text{ km}$ ) planetesimals.

For the default model, we assume that both Jupiter and Saturn have already obtained their present-day masses. During the passage of  $\nu_5$  and  $\nu_6$ , planetesimal eccentricity excitation occurs due to angular momentum transfer from these smaller bodies to Jupiter and Saturn (without any energy exchange). The strength of the torque is a function of Jupiter's and Saturn's eccentricities ( $e_J$  and  $e_S$ , respectively). These quantities also oscillate with an amplitude that is determined by the total angular momentum deficit of the system, i.e., the difference between the actual sum of Jupiter's and Saturn's angular momentum and the maximum values for their given semimajor axes ( $a_J$  and  $a_S$ , respectively).

Since Jupiter's mass is substantially larger than that of Saturn, it is adequate to specify the angular momentum deficit of the system by assigning an initial non-zero eccentricity,  $e_J$  to Jupiter only. While Saturn is initialized with a circular orbit, its eccentricity is rapidly excited by Jupiter. In principle, we can adopt the initial value of  $e_J$  from the current angular momentum deficit of the solar system, or from the results of other numerical simulations. However, the angular momentum deficit of the system may have evolved due to the gas giants' interaction with residual planetesimals and gas. Taking these uncertainties into account, we consider two values for Jupiter's initial eccentricity, which are slightly larger and slightly smaller than Jupiter's present-day value, respectively. In the next section we discuss the consequences of these choices for  $e_J$ .

### 3.2. Contribution of gravity and damping by the gas disk

We mainly focus on the advanced stage of nebula evolution when the giant planets' gas accretion is quenched by gap formation and type II migration is stalled by the depletion of the disk gas (Lin & Papaloizou 1986; Dobbs-Dixon et al. 2007). In our model we assume (i) a thin-disk approximation, (ii) an asymmetric power-law surface density distribution based on the MMSN model (Hayashi 1981), with (iii) an axisymmetric gap near the gas giant (Bryden et al. 1999), and (iv) that all planetary components (gas giants and planetesimals) are coplanar in the protoplanetary disk.

We adopt a thin-disk model with an axisymmetric surface density distribution,  $\Sigma(r, t)$ , of the form

$$\Sigma(r, t) = \Sigma(r_0, 0) f_{\text{dep}}(t) (r/r_0)^{-k}, \quad (1)$$

where  $r_0 = 1 \text{ AU}$  and  $f_{\text{dep}}(t) = \exp(-t/T_{\text{dep}})$  is the time-dependent depletion function of the gas disk. In the MMSN model,  $k = 1.5$  is widely used with an initial surface density  $\Sigma(r_0, 0) = 1700 \text{ g/cm}^2$  at the location of  $r_0 = 1 \text{ AU}$ . We approximate the density of the residual gas to be  $\rho_g = \Sigma(r, t)/H(r)$ , with a disk scale height that has a similar form to that in the work of Hayashi (1981) and Thommes et al. (2008), but is reduced by a factor of two:

$$H(r) = 0.025 \left( \frac{r}{1 \text{ AU}} \right)^{5/4} \text{ AU} \quad (2)$$

(see further discussions in §4.4.1). This relatively small thickness is appropriate for the advanced stages of disk depletion (Garaud & Lin 2007).

The characteristic decay time scale is chosen to be  $T_{\text{dep}} = 1 \text{ Myr}$  for the default models. The initial time ( $t = 0$ ) is set to be the start of gas depletion (rather than the epoch of CAI formation). This definition is consistent with the assumed prior emergence of Jupiter at the onset of our computation. In comparison with observational data,  $T_{\text{dep}}$  corresponds to the duration for transition from classical to weak-line disks. This time scale may be somewhat shorter than the average age of stars with detectable IR excess in their continuum spectral energy distribution, though it is comparable to the observationally inferred evolutionary time scales for transitional disks (Currie & Sicilia-Aguilar 2011). Although the detailed dynamical evolution of the residual planetesimals may depend on the chosen model parameters, including the functional forms of  $\Sigma(r, t)$  and  $T_{\text{dep}}$ , this working disk model provides an adequate set of initial conditions to generate several illustrative examples.

We compute the disk gravity on the gas giants (Jupiter and Saturn) and the planetesimals separately, because the apsidal precession of the planetesimals by the gas disk is dominated by the gas in their neighborhood, whereas the gas giants' apsidal precession caused by disk gravity is sensitive to the gap structure (Nagasawa et al. 2005). Gas giants that have opened a gap experience a gravitational force that depends on the locations of the inner and outer boundary of the gap (Ward 1981; Nagasawa & Ida 2000):

$$F(r, t) = 2\pi G \Sigma(r, t) \sum_{n=0}^{\infty} A_n \left\{ \left( \frac{2n}{2n-1+k} \right) \left( \frac{r}{R_{\text{out}}} \right)^{2n-1+k} - \left( \frac{2n+1}{2n+2-k} \right) \left( \frac{R_{\text{in}}}{r} \right)^{2n+2-k} \right\}. \quad (3)$$

Several models are presented here. In all models, we set the semimajor axis of Jupiter to its present-day value (5.2 AU) and  $R_{\text{in}} = 4.5 \text{ AU}$  in accordance with the results of numerical simulations (Bryden et al. 1999). In the



default model and several other models, we also set Saturn’s semimajor axis to its present-day value (9.58 AU) and adopt  $R_{\text{out}} = 11.0$  AU following the results of numerical simulations (Bryden et al. 2000). In all models we find that the dynamical evolution of Jupiter’s and Saturn’s orbits and the propagation of the  $\nu_5$  and  $\nu_6$  SRs depend sensitively on  $R_{\text{in}}$  and weakly on  $R_{\text{out}}$ . For computational convenience, we adopt the same values of  $R_{\text{in}}$  and  $R_{\text{out}}$  in all models presented here.

The effect of gravity on the planetesimals is more complex. Even though the gravity experienced by the planetesimals is usually dominated by bodies in the nearby region, planetesimals in the region close to the inner edge ( $R_{\text{in}}$ ) of the truncated disk are also affected by the presence of the gap. We therefore combine the prescription constructed in Nagasawa et al. (2005) with the “gap effect” of Ward (1981) to compute the disk’s gravity on the planetesimals located at radius  $r$ . We find

$$F = -4\pi G \Sigma(r, t) \left\{ Z_k + \sum_{n=0}^{\infty} A_n \left( \frac{n}{2n-1+k} \right) \left( \frac{r}{R_{\text{in}}} \right)^{2n-1+k} \right\}. \quad (4)$$

While MMRs and SRs excite the orbits of planetesimals, residual gas in the nebula also damps the eccentricity of the planetesimals. For small (sub-kilometer-size) planetesimals, this process operates mainly through hydrodynamic drag (Adachi et al. 1976). For large (super-moon-size) embryos, the main eccentricity-damping mechanism is planet-disk tidal interaction (Goldreich & Tremaine 1980; Ward 1997). Whereas the SRs remove angular momentum and preserve the energy of planetesimal orbits, eccentricity damping leads to the dissipation of energy without changes in the angular momentum of their orbits. Consequently, planetesimals undergo inward migration during orbital circularization. For those planetesimals whose eccentricities are damped efficiently, the orbital decay is kept in pace with the inward propagation of the  $\nu_5$  SR. These planetesimals “surf” over extended radial distances.

With a simple approximation (Zhou et al. 2007) we compute the effect of eccentricity damping with a drag force that reduces the amplitude of the planetesimals’ epicyclic motion around their guiding centers such that

$$\mathbf{F}_D = -\frac{\mathbf{V} - \mathbf{V}'_{\text{kep}}}{T_{\text{damp}}}. \quad (5)$$

In this expression, the motion of the gas is assumed to be axisymmetric and in the azimuthal direction with an amplitude  $V'_{\text{kep}} = V_{\text{kep}}(1 - \eta)$ , where the dimensionless parameter  $\eta \approx (c_s/4V_{\text{kep}})^2$ , with  $c_s$  as the sound speed, represents the contribution from the pressure gradient (Adachi et al. 1976).

The magnitude of  $T_{\text{damp}}$  is different for the small and large planetesimals. The eccentricities of small planetesimals are mainly damped by hydrodynamic drag. Since the planetesimal radii  $r_p$  are much larger than the molecular mean free path in the gas, the Stokes drag law (Whipple 1972; Adachi et al. 1976; Weidenschilling 1977; Ida & Lin 1996; Supulver & Lin 2000) can be applied in our model, and it operates on a timescale

$$T_{\text{damp,s}} = \frac{1}{C_D} \frac{\rho_p}{\rho_g} \frac{r_p}{V_{\text{rel}}} \simeq \frac{43}{f_{\text{dep}}} \left( \frac{\rho_p}{1 \text{ g/cm}^3} \right) \left( \frac{r_p}{1 \text{ km}} \right) \left( \frac{a}{1 \text{ AU}} \right)^{11/4} \left( \frac{V_{\text{rel}}}{1 \text{ km/s}} \right)^{-1} \text{ yr}, \quad (6)$$

where  $\rho_p$  is the internal density of the planetesimals,  $V_{\text{rel}} = V - V'_{\text{kep}}$  is the relative velocity between gas and asteroids. This expression has a factor of 3/8 discrepancy from that in Whipple (1972), and in the limit of a large Reynolds number, the drag coefficient is  $C_D = 0.165$ .

The eccentricity of large embryos is damped by the torque associated with their tidal interaction by the disk gas at their Lindblad resonances (Ward 1989, 1993; Artymowicz 1993; Thommes et al. 2008) on a time scale

$$T_{\text{damp,t}} \simeq \left( \frac{M_*}{M_p} \right) \left( \frac{M_*}{\Sigma a^2} \right) \left( \frac{H}{a} \right)^4 \Omega_k^{-1} \simeq \frac{3 \times 10^{-4}}{f_{\text{dep}}} \left( \frac{M_p}{M_{\odot}} \right)^{-1} \left( \frac{a}{1 \text{ AU}} \right)^2 \text{ yr}. \quad (7)$$

In addition, the corotation torque (e.g., Paardekooper et al. 2011) also contributes to the eccentricity damping. The corotation torque has a similar dependence on the surface density and temperature distribution in the disk and a magnitude that is a few times larger than the Lindblad torque. For simplicity, we artificially enhance the total tidal damping from the expression in Equation (7) by a factor of five. Note that  $T_{\text{damp,t}} \propto M_p^{-1}$ , so that the efficiency of tidal damping increases with the mass of the planetesimals and embryos.

As the efficiency of eccentricity damping decreases over time, the locations of the  $\nu_5$  and  $\nu_6$  SRs move inward as the solar nebula is globally depleted over several  $T_{\text{dep}}$ . Nevertheless, the combined effect of the mechanisms described above can clear a large fraction of the residual planetesimals from the main asteroid belt region. After  $t > 10 \times T_{\text{dep}}$ , gas is severely depleted in the disk and the  $\nu_5$  SR passes through the present-day orbit of Mars. The concentration of planetesimals around 1–2 AU increases, and as a result, their collisional probability increases. Based on the results of their numerical simulations, Thommes et al. (2008) suggest that the associated giant impacts may have promoted the final assemblage of the Earth and Mars, as well as the giant impact that has led to the formation of the Moon.

The chronology of this scenario is consistent with the age estimate of the Earth based on radiogenic dating of Hafnium isotopes (Kleine et al. 2009).

#### 4. NUMERICAL RESULTS

##### 4.1. *SR sweeping*

For our fiducial models we adopt Jupiter’s present-day eccentricity  $e_J = 0.05$  as our initial condition. The embedded planetesimals are initialised with a semimajor axis distribution

$$dN/da \propto a^{-1.5} \quad (2.0 \text{ AU} \leq a \leq 3.5 \text{ AU}) . \quad (8)$$

The contribution of the hydrodynamic drag and the planetesimal-disk tidal interaction imply that the total damping efficiency is closely correlated with the size of the planetesimals.

Figure 1 shows how the sweeping SR clears planetesimals from a representative primordial location (3 AU). We consider four representative cases. The left panels show the results for small (10 km) and large (1000 km) planetesimals, which are significantly influenced by gas drag and type I damping, respectively. The right panels present the results for intermediate-size planetesimals (300 and 500 km). The efficiency of eccentricity damping for the intermediate-size planetesimals is lower than both the small and the large planetesimals.

At the early stage of evolution, the small and large planetesimals (left panels in Fig. 1) undergo inward migration due to hydrodynamic and type I tidal drag, respectively. In contrast, the intermediate-size planetesimals preserve their initial semimajor axes (right panels). The  $\nu_5$  and  $\nu_6$  SRs sweep through this region after  $\sim 2T_{\text{dep}} - 4T_{\text{dep}}$  and all the planetesimals experience a rapid eccentricity excitation. Efficient eccentricity damping causes the 10 and 1000 km sized planetesimals to undergo considerable inward migration. Due to the relatively low eccentricity-damping efficiency, a fraction of the planetesimals with intermediate sizes remain near their initial locations. However, most of them are also lost from the main belt region. The retention probability is determined by the planetesimals’ orbital phase during the SRs’ passage through their semimajor axis. The retained planetesimals have modest residual eccentricities.

Based on these results, we infer that (i) nearly all planetesimals larger than the Moon or smaller than  $\sim 10$  km are likely to undergo extensive orbital decay and are evacuated from 3 AU and (ii) some, but not all, intermediate-size asteroids may survive the passage of the  $\nu_5$  and  $\nu_6$  SRs and retain their initial semimajor axis at 3 AU. These outcomes provide a potential explanation for the depletion and size selection of residual planetesimals from the asteroid main belt region.

In order to generalize the results above, we consider other initial  $a_p$  values for two groups of planetesimals, according to their sensitivity to orbital damping: (i) the strong-damping class and (ii) the weak-damping class. For the strong damping class, we take planetesimals of size 10 km as a representative case. Figure 2 shows the evolution of the semimajor axis, perihelion, and aphelion distances, starting with four different initial semimajor axes,  $a_p = 3.5$  AU,  $a_p = 3.2$  AU,  $a_p = 2.7$  AU, and  $a_p = 2.3$  AU. These locations cover the entire region of interest. After time  $t = 10T_{\text{dep}}$ , all four representative planetesimals have undergone orbital decay to regions closer to the Sun than the main belt region.

Within  $\sim 0.2T_{\text{dep}}$ , hydrodynamic drag leads to a fractional orbital decay for the planetesimals initially located at 3.5 AU. As these planetesimals pass through Jupiter’s and Saturn’s MMRs and SRs, their eccentricities are excited. Subsequent eccentricity damping leads to orbital decay. Provided that  $a_J$  remains constant, the location of the MMR is fixed. In the region close to Jupiter ( $\gtrsim 3$  AU), its low-order (especially 2:1) MMRs are primarily responsible for the excitation and subsequent inward migration of planetesimals (Ida & Lin 1996).

Closer to the Sun, however, the torque induced by higher-order MMRs is limited by the small magnitude of  $e_J$ . The planetesimals’ eccentricity excitation and orbital evolution are dominated by the SRs. During disk depletion, the locations of the  $\nu_5$  and  $\nu_6$  SRs are relocated closer to the Sun. It is therefore possible for some planetesimals to be continually excited by the evolving SRs. After  $\sim 5T_{\text{dep}}$ , there is little residual gas left in the disk to induce any significant (i) precession for Jupiter or Saturn and (ii) eccentricity damping for the planetesimals. Consequently, the propagation of the  $\nu_5$  and  $\nu_6$  SRs is stalled inside the orbit of Venus and outside the orbit of Mars, respectively. The planetesimals also retain their eccentricities.

The contributions of the MMRs and SRs can be distinguished by the evolution of the planetesimals’ semimajor axis and eccentricity. The planetesimal semimajor axes evolve through several low-order MMRs, including the 5:2, 3:1, and 4:1 MMRs. In the limit of small  $e_J$ , the passages through these other MMRs (apart from the powerful 2:1 MMR) do not lead to strong eccentricity excitation and significant planetesimal migration. Nevertheless, the planetesimals’ response to the 3:1 and 4:1 MMRs is enhanced when the passage is partly coupled with the propagation of the  $\nu_5$  and  $\nu_6$  SRs.

For planetesimals in the weak-damping class, the situation is somewhat different from the strong-damping class (see Fig. 1). In Figure 3, we show the orbital evolution of planetesimals in the weak-damping class with a representative size,  $r_p = 100$  km. These planetesimals’ orbits evolve under the combined effect of MMRs and the sweeping secular resonance. Figure 3 shows how the  $\nu_5$  and  $\nu_6$  SRs sweep through the main belt region. We compare the analytical

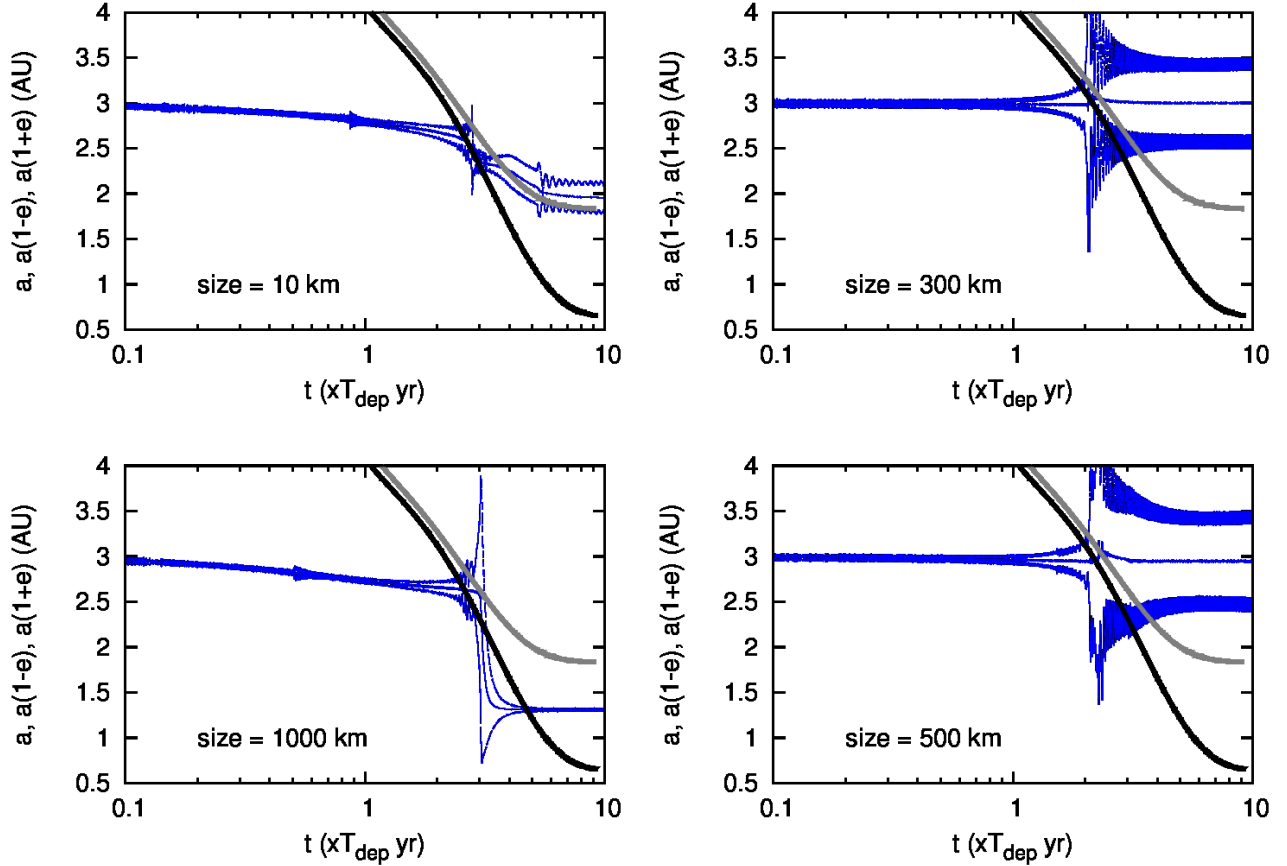


**Figure 1.** Perihelion, semimajor axis and aphelion evolution for four representative planetesimals (with  $r_p = 10, 300, 500$ , and  $1000$  km). In all cases, the initial semimajor axis is  $a_p = 3$  AU. The black and gray curves refer, respectively, to the locations of the  $\nu_5$  and  $\nu_6$  SRs obtained from analytic calculations.

solutions for  $\nu_5$  (black arrow) and  $\nu_6$  (grey arrow) SRs with the numerical results of §3.1. Orbital excitation occurs between 2.9 AU and 2.1 AU, and eccentricity variations are consistent with the analytical predictions for the  $\nu_5$  and  $\nu_6$  SRs. The only exception is the case where the planetesimals are initially located beyond 3 AU ( $a_p = 3.3$  AU), this region is dominated by the extended 2:1 MMR, and these planetesimals are excited prior to the passage of the SSR.

We can therefore infer that the original location of planetesimals in the main belt region determines whether their excitation is dominated by either the MMR or by the sweeping SR, irrespective of the rate of eccentricity damping they experience. In general, the MMR plays a key role in exciting the eccentricity for planetesimals with initial  $a_p \gtrsim 3$  AU, while for those with initial  $a_p \lesssim 3$  AU, the  $\nu_5$  and  $\nu_6$  SRs are mainly responsible for their angular momentum deficit.

#### 4.2. Asteroid size selection

The observed present-day SFD in the main asteroid belt appears to have a transition at around  $r_p \approx 50$  km (e.g., Bottke et al. 2005; Morbidelli et al. 2009). This transition has been interpreted in terms of a cutoff in the population of small asteroids shortly after their formation. Such an initial SFD may either be attributed to either the preferential formation of large asteroids or the clearing of small embryos due to a sweeping SR. In this work, we presume that the existence of a protoplanetary disk undertakes the natural selection role, rather than invoking a new formation mechanism. In this scenario there are two key processes at play: (i) planetesimals in the main asteroid belt region can be significantly excited as SRs (in this work the  $\nu_5$  and  $\nu_6$  SRs) propagate through the region; and (ii) the excited planetesimals experience dispersive inward migration due to the size-dependent eccentricity damping force.

In Figure 4, we show this dependence for an assumed initial size distribution  $N(r_p) \propto r_p^{-1}$ , for a set of representative planetesimals with sizes in the range of 10 – 1000 km. In order to illustrate the size dependence on the two damping mechanisms, we analyze the efficiency of these effects separately. The contribution from the hydrodynamic drag decreases as  $T_{\text{damp}}/T_{\text{dep}} \propto r_p$  whereas that from the tidal damping follows  $T_{\text{damp}}/T_{\text{dep}} \propto r_p^{-3}$  (see eqs. 6 and 7, respectively). Using these proportionalities, we estimate the combined effect of these two damping mechanisms. The solid black curve shows the damping at  $t = 0.01T_{\text{dep}}$ , and the dashed black curve indicates the result at the end of the simulation ( $t = 10T_{\text{dep}}$ ). Most interesting, the “bump” that corresponds the weak-damping class shifts to larger-size

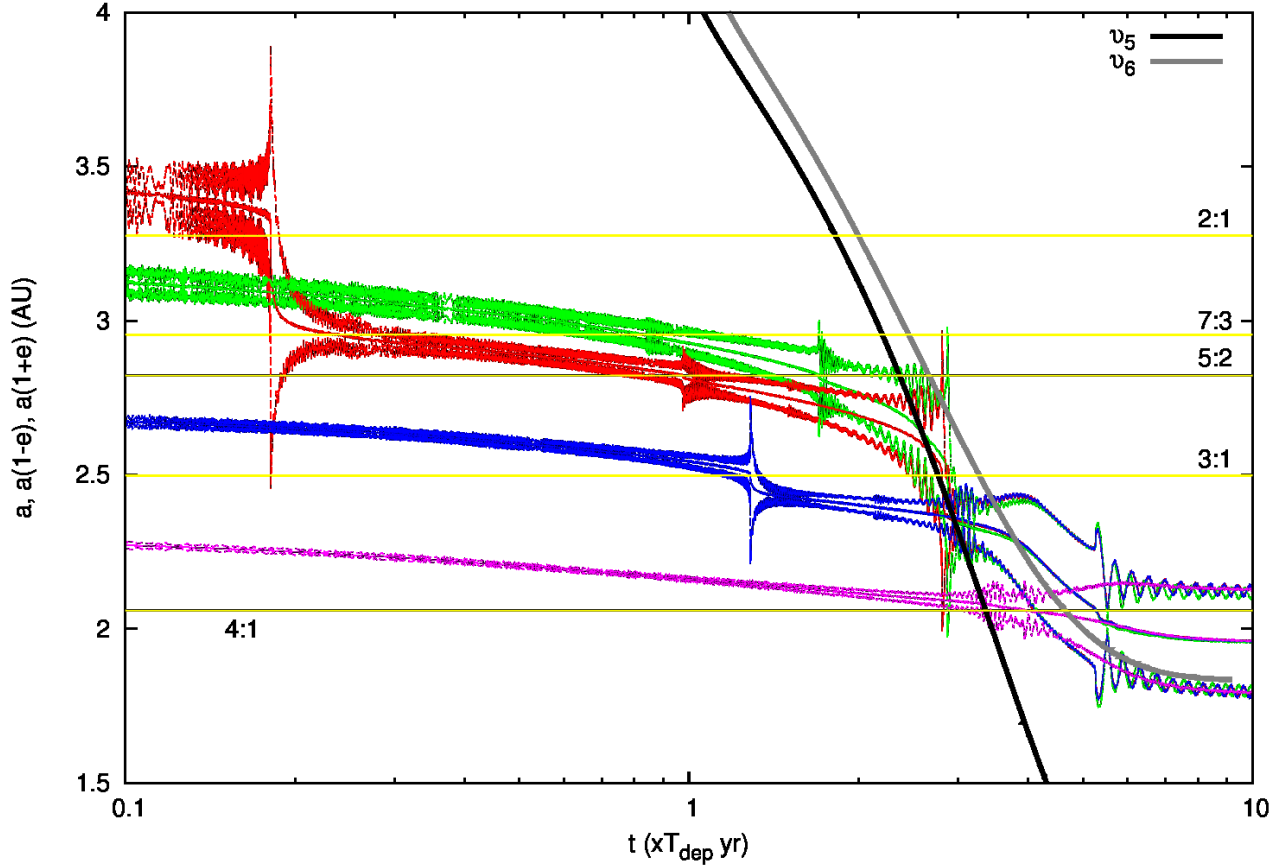


**Figure 2.** The evolution of the perihelion, semimajor axis and aphelion of 10 km size planetesimals. The black and gray curves represent the analytical location of the  $\nu_5$  and  $\nu_6$  SRs, respectively. The yellow lines show the locations of several of Jupiter’s low-order MMRs.

planetesimals during the disk depletion.

A default model  $A_1$  is introduced with an initial SFD of the form  $N(r_p) \propto r_p^{-3.5}$ . While the shape of this SFD is retained for the intermediate-size ( $300 \text{ km} \lesssim r_p \lesssim 1000 \text{ km}$ ) planetesimals, the smaller ( $r_p \lesssim 50 \text{ km}$ ) bodies are severely cleared during the phase of gas depletion. The final normalized SFD (at  $T = 10T_{\text{dep}} = 10 \text{ Myr}$ ) in the main belt region ( $\sim 2.1 - 3.3 \text{ AU}$ ) is shown in Figure 5. Although the final distribution does not completely match the observed SFD, it demonstrates the possibility of preferential retention of relatively large planetesimals. The observed size distribution of the small known asteroids can be produced from the subsequent collisional fragmentation process. There are several families of asteroids that bear the signature of collisional fragmentation (Zappala et al. 2002; Nesvorný et al. 2006).

#### 4.3. Mass depletion in the primordial asteroid belt

The size dependence of the drag force for eccentricity damping leads to differential inward migration rates. Moreover, the size range for effective eccentricity damping (i.e., those planetesimals with  $T_{\text{damp}}/T_{\text{dep}} < 1$ ) evolves with time. The asymptotic retention efficiency (in the main belt) indicates that all the planetesimals with  $r_p \lesssim 50 \text{ km}$  and  $r_p \gtrsim 1000 \text{ km}$  are cleared and only a small fraction of intermediate-size planetesimals are retained (Fig. 6). These results show that throughout the main belt region, (i) most of the planetesimals (99.9 % in their total mass) are cleared and (ii) the residual planetesimals have a size distribution similar to that of the observed SFD of asteroids larger than  $r_p \approx 50 \text{ km}$ .

The default model  $A_1$  also predicts a substantial migration of the planetesimals with initially  $a_p = 2 - 3.5 \text{ AU}$  to the region interior to the present-day orbit of Mars (1.5 AU). Using the prescription for the evolution of the disk surface density distribution in the default model  $A_1$ , the semimajor-axis evolution of planetesimals with  $r_p = 10 - 1000 \text{ km}$  is plotted in Figure 9. A large fraction of this population undergoes orbital decay as the  $\nu_5$  and  $\nu_6$  SRs propagate inward and excite their eccentricities, which are subsequently damped by the residual disk gas. As we indicated above, the decrease in the planetesimals’ semimajor axes is due to the combined effects of Jupiter’s secular perturbation and eccentricity damping by the disk, provided that the orbital decay time scale  $\tau_a = a/\dot{a} = -\tau_e(1 - e^2)/2e^2$  is shorter than the  $\nu_{5,6}$  SRs’ propagation time scale,  $\tau_{\nu_{5,6}} \sim \tau_{\text{dep}}$ . Therefore, after  $t \approx 6T_{\text{dep}}$ , although  $\nu_{5,6}$  SRs continue to move



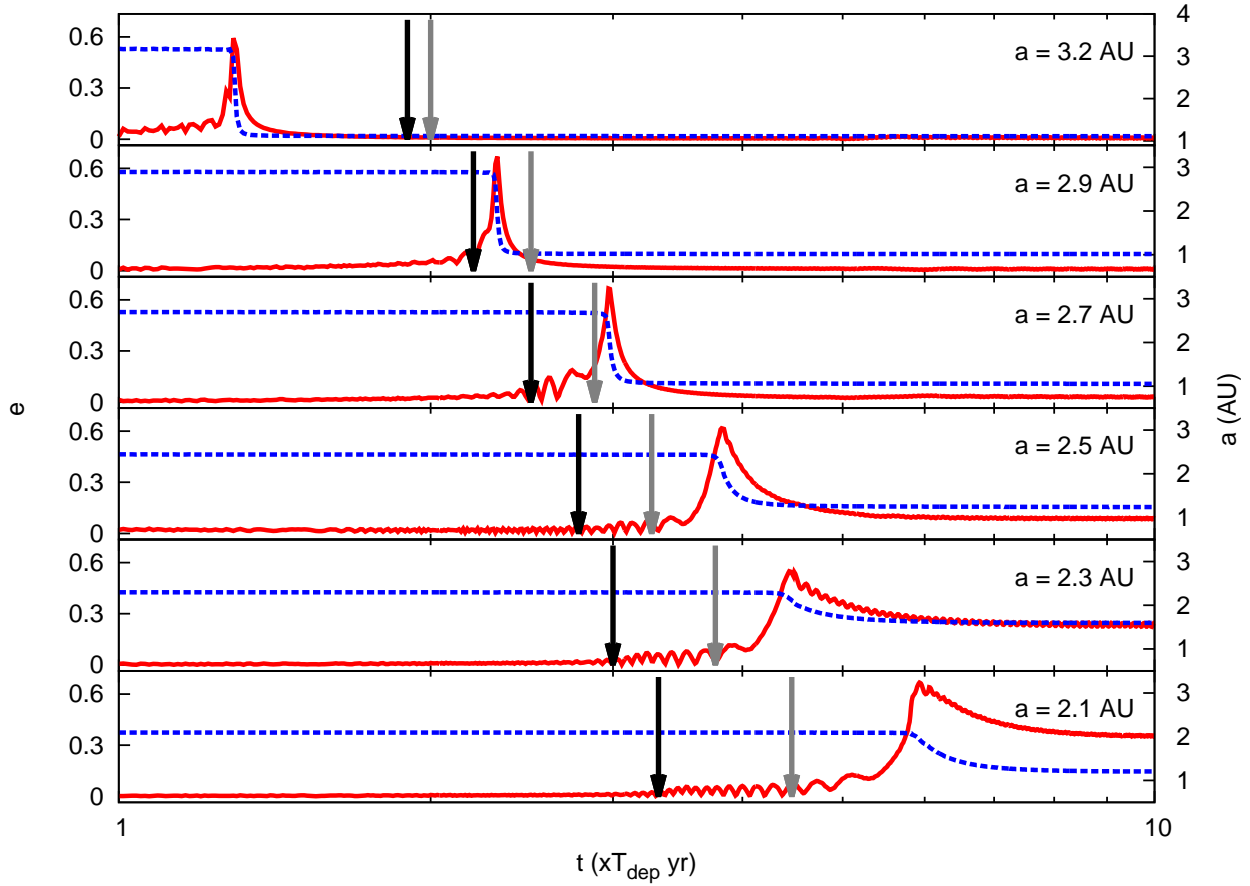


**Figure 3.** Eccentricity (red) and semimajor axis (blue) evolution for planetesimals with  $r_p = 100$  km. The black/gray arrows indicate the epoch of the  $\nu_5/\nu_6$  SR passage.

inward, most of the planetesimals become detached from the SR recapture.

We also discuss the asteroids' eccentricity distribution. In the absence of Jupiter's perturbation and gas drag, the residual planetesimals may establish a collisional equilibrium with a velocity dispersion comparable to a fraction of the surface escape speed of the largest members (Aarseth 1993; Palmer et al. 1993; Kokubo & Ida 1998). If the asteroids' observed eccentricity distribution (up to  $e = 0.4$ ) was established through their mutual dynamical interaction, it would require dynamical stirring by a population of large ( $> 1000$  km) embryos that must be cleared out from the asteroid belt.

The SSR can lead to the clearing of these large embryos. Moreover, it can also excite and preserve modest eccentricity for the retained planetesimals. In Figure 7 we plot the asymptotic eccentricities of the surviving planetesimals as a function of their  $r_p$  and  $a_p$  in the main belt at time  $t = 10T_{\text{dep}}$ . As shown above, the surviving planetesimals are mainly concentrated in the size range from 100 km to 1000 km, which belongs to the weak-damping group. As the eccentricities of most of these planetesimals are excited by the SSR, their damping timescale is generally longer than the gas disk depletion timescale (see also Fig. 1). Most of the planetesimals only experience modest orbital decay and maintain an eccentricity distribution with a considerable dispersion and an average value of  $e \sim 0.2$ , which is comparable to the observed distribution. However, there are several extremely excited cases ( $e > 0.6$ ) around  $a_p \approx 2.1 - 2.3$  AU. These planetesimals are able to retain their high eccentricities because when the  $\nu_{5,6}$  SRs sweep through this region after  $\sim 5 - 6$  Myr (see also Fig. 9), most of the gas material is severely depleted, so that eccentricity damping becomes inefficient. These highly eccentric planetesimals cross the orbits of Mars, and they are likely to be destabilized and ejected from this region.

The results in Figure 7 indicate that the eccentricities of the asteroids in the main belt may indeed be due to excitation by the SSRs of Jupiter and Saturn. In contrast, the present-day inclination distribution of main belt asteroids cannot be fully attributed to the same mechanism. Although Jupiter's and Saturn's sweeping vertical SR (due to the matching of nodal precession rates during the nebula's depletion) can excite the inclination of some planetesimals, the magnitude of this effect is too weak to account for the observed inclination distribution of asteroids in the main belt (Heppenheimer 1980; Ward 1981; Nagasawa et al. 2000). Instead, we consider the possibility that

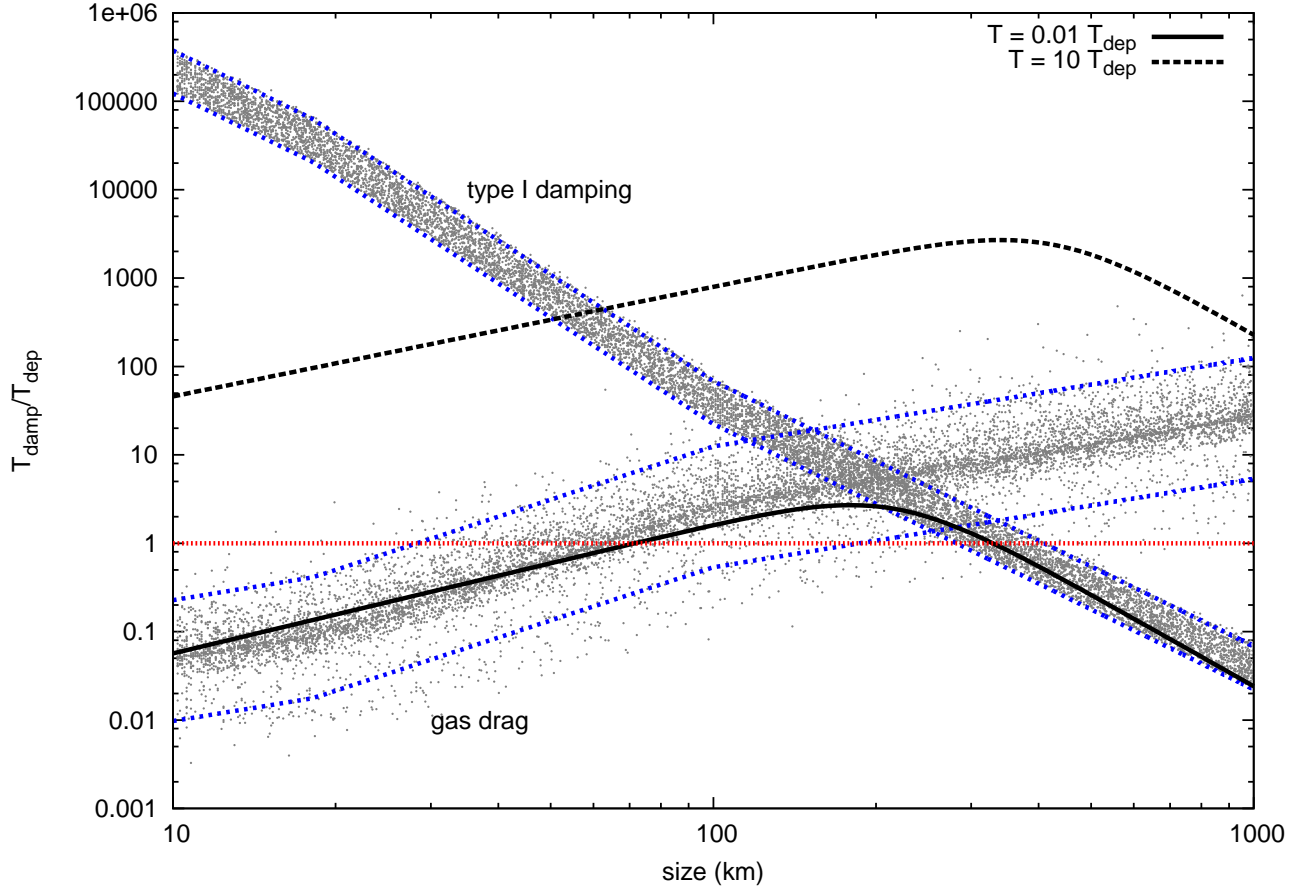


**Figure 4.** Eccentricity damping time (in units of the disk depletion time scale) versus planetesimal radius. The two mechanisms for eccentricity damping are computed independently. When their contribution is combined, the eccentricities of the planetesimals are damped on the minimum  $T_{\text{damp,tot}}$  time scale ( $T_{\text{damp,tot}} = (1/T_{\text{damp,s}} + 1/T_{\text{damp,t}})^{-1}$ ). The black dots are the simulated results, while the blue dashed curves are obtained from analytical fits. The red dashed curve refers to the critical value that distinguishes effective and ineffective eccentricity damping processes.

eccentricity excitation by SSRs induces planetesimals to undergo frequent orbit crossings, and that their inclinations were subsequently excited to their observed values by their mutual perturbations and close encounters.

In order to verify the possibility, we extend our default model with 100 massless planetesimals plus several large embryos (sizes ranging between 1000 and 3000 km), with semimajor axis randomly placed between 2.1 and 3.3 AU. We take into account embryos' gravitational perturbation on the planetesimals as well as each other. For these intermediate-size planetesimals, inclination damping due to hydrodynamic and tidal drag is neglected. Each of these planetesimals and embryos is assigned with a small initial non-zero inclination, randomly chosen from a uniform distribution between  $i = 0^\circ$  and  $i = 5^\circ$ . We carried out 10 sets of simulations. The inclination distribution of our simulated models is compared with the asteroids' present-day inclination distribution. The results in Figure 8 support our conjecture that although most large embryos are cleared out of the main belt region by Jupiter's and Saturn's SSRs, the inclination of the retained planetesimals can be excited well above their initial values during the migration process, to values comparable to that observed among the asteroids. A sizeable fraction of planetesimals retains their initial small inclination. This fraction would be reduced if more embryos were included in each run so that the frequency of close encounters may be enhanced. We have neglected the effect of nodal precession for Jupiter, Saturn, embryos, and planetesimals. These effects may enhance the inclination excitation for the planetesimals. Similar to the results in Figure 7, there is a population of substantially inclined planetesimals at  $a_p \approx 2.1 - 2.3$  AU. After the disk gas has been severely depleted, the orbits of these highly inclined planetesimals may be destabilized due to perturbations by Mars.

In Figure 9 we trace the migration of  $10^4$  planetesimals and find that the SR starts outside of 3.5 AU, which is outside the current outer boundary of the main asteroids belt, and then sweeps through the entire main belt region. Therefore, nearly all the planetesimals in the main belt are affected by the  $\nu_{5,6}$  SRs as they sweep through the region. In general, this process results in two possible outcomes. First, if their initial semimajor axes are close to that of Jupiter, the planetesimals start out in the gap around the planet. In this limit, Jupiter's and Saturn's secular perturbations are

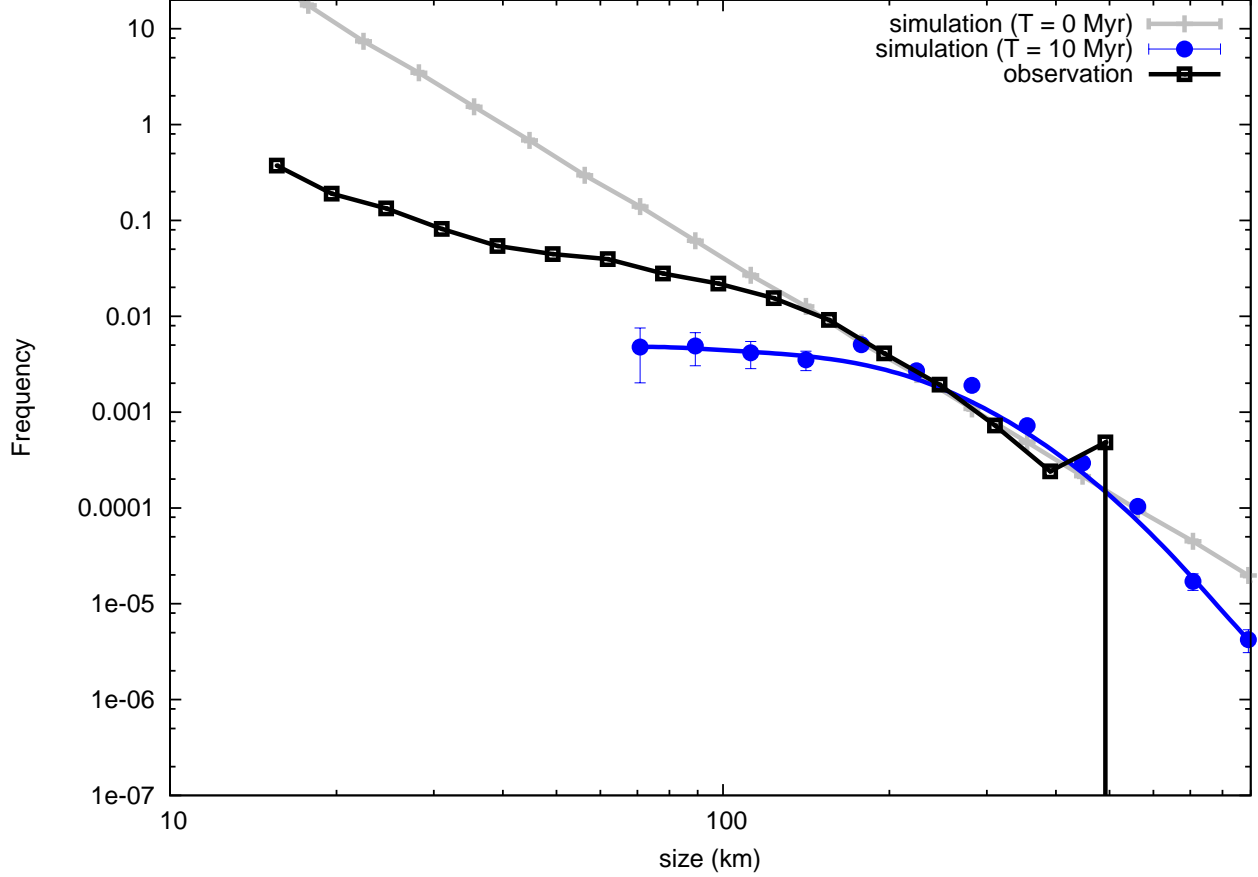


**Figure 5.** Observed SFD and the asymptotic SFD from our default model  $A_1$  in the main belt region ( $\sim 2.1 - 3.3$  AU). The observational data (black curves) are obtained from Bottke et al. (2005). The initial ( $t = 0$  Myr; gray plus signs) and asymptotic ( $t = 10$  Myr; blue dots) normalized SFDs are adjusted to fit the observed SFD at  $r_p = 200$  km.

strong and the damping efficiency is due to the relatively low surface density of the disk. Planetesimals in the gap region are then scattered away from the gas giants. Some planetesimals are scattered toward the inner parts of the solar system where the eccentricity damping efficiency is high. These planetesimals then follow the propagation of the  $\nu_{5,6}$  SRs. A small fraction of the asteroids may be able to avoid being captured by the sweeping SRs and retain their initial location in the main asteroid belt. These are the planetesimals that are located relatively far from Jupiter’s zone of influence and are in the “preferred” size range.

#### 4.4. Model parameters

All the results discussed in the previous sections are based on our default model  $A_1$ . In this section we briefly discuss how our choices for the initial conditions and the boundary conditions may influence the final SFDs of the asteroids, and additional observations can also help us to put further constraints on the properties of the young solar system.

##### 4.4.1. Dependence on the gas disk

In our disk models, we follow the widely adopted MMSN prescription in which

$$H = h_0 \left( \frac{r}{1 \text{ AU}} \right)^{5/4} \text{ AU} . \quad (9)$$

This result is based on the assumption that gas can establish local thermal equilibrium with the solar irradiation everywhere in the disk. In the original MMSN model (Hayashi 1981), this assumption leads to  $h_0 = 0.05$ . This assumption is likely to be satisfied after the disk becomes optically thin so that most super-micron dust grains and planetesimals are directly exposed to the solar radiation. It also requires these dust particles to be thermally coupled to the gas.

However, the inner parts of the solar nebula, including the main belt region, may remain opaque to stellar photons even when the surface density of the dust grains in these regions is substantially, but not severely, depleted from that of the MMSN. In this limit, the gas temperature is determined by both viscous dissipation near the opaque midplane

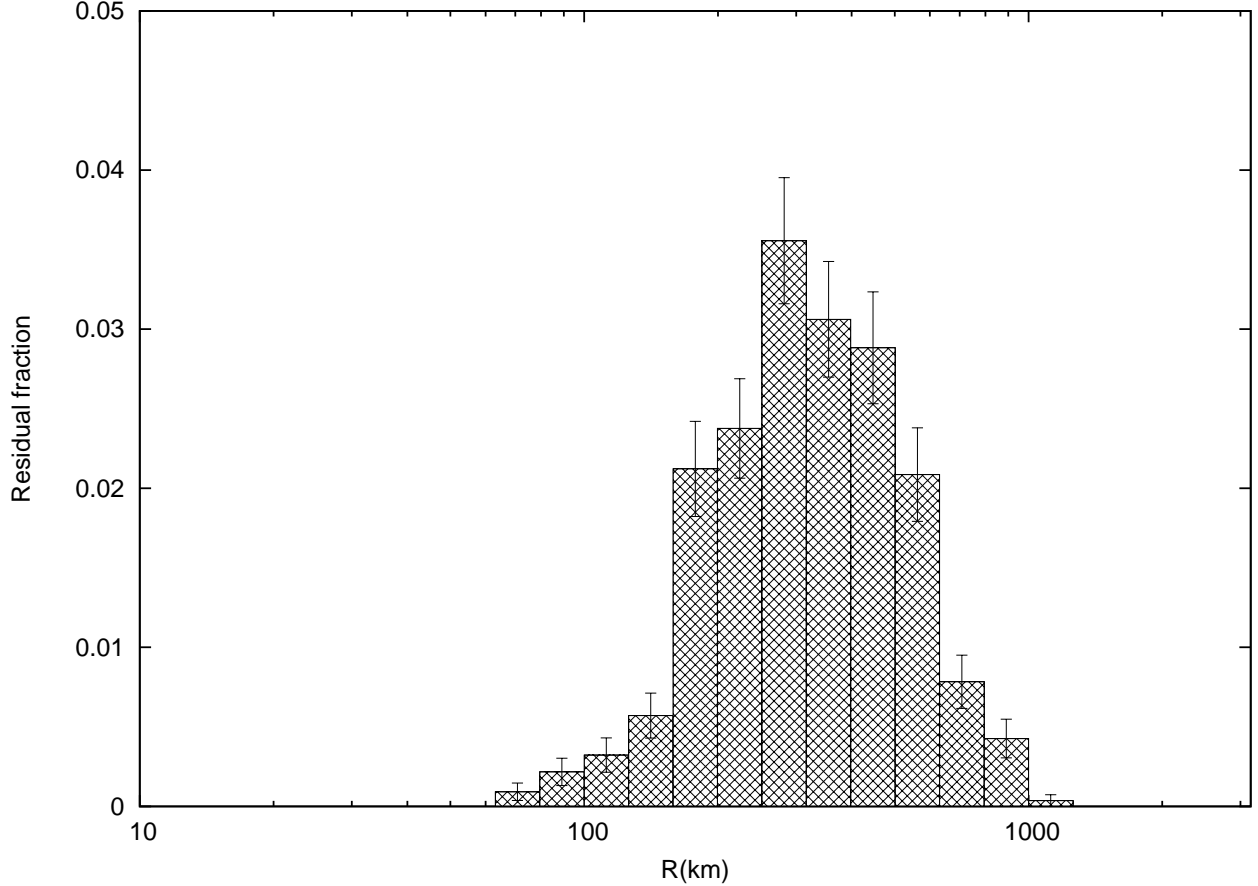


**Figure 6.** Residual fraction of planetesimals in the main belt ( $\sim 2.1 - 3.3$  AU) as a function of planetesimal size  $r_p$  at time  $t = 10T_{\text{dep}}$ , for the default model  $A_1$ .

and stellar irradiation on the exposed dust in the optically thin surface layer of a flared nebula. [Garaud & Lin \(2007\)](#) took these effects into account and constructed models with radial dependence in the disk thickness and smaller values of  $h_0$ .

In our default model  $A_1$ , we adopt  $h_0 = 0.025$ , which is appropriate for the advanced stages of disk evolution when the main belt region remains opaque. In order to consider the possibility that the disk may have become optically thin, due to dust coagulation and planetesimal formation, we also simulated model  $A_2$  with the conventional value of  $h_0 = 0.05$ . We compare the results of these two models to evaluate the dependence of  $h_0$  on the asymptotic SFD in the main belt region (Fig. 10). Since  $T_{\text{damp},t} \propto H^4$  (eq. 7) and  $T_{\text{damp},s} \propto H$  (eq. 6), a modification of the scale height factor,  $h_0 \propto H$ , significantly changes the damping efficiency. This dependence is particularly sensitive for type I damping, and it results in different mass depletion fractions, as well as in a different asymptotic SFD. As  $h_0$  is doubled from model  $A_1$  to model  $A_2$ , five times more residual planetesimals are retained in the the main asteroid belt region. Moreover, the “bump” in the residual planetesimals’ size distribution also shifts from  $\approx 300$  km (in model  $A_1$ ) to  $\approx 600$  km (model  $A_2$ ). This model dependence is the result of the tidal damping mechanism for large planetesimals, which is most strongly influenced by the value of  $h_0$ .

The average time scale for the infrared and millimeter excess to decrease below the detectable threshold is 3-5 Myr ([Haisch et al. 2001](#)). These features are signatures of dust, not gas. Observational data also indicate a wide dispersion in the disk fading time scale (ranging from 1 to 10 Myr) even among coeval stars within the same young stellar clusters ([Zuckerman et al. 1995](#)). The gas depletion time scale ( $T_{\text{dep}} = 1$  Myr) in the default model is on the low end of the observed IR persistent time scales, although it is comparable to the shorter time scale inferred for the transition from classical to weak-line disks. Here we consider the possibility of somewhat longer gas depletion time scales. In Figure 10, we compare the results of the default model  $A_1$  to those with a gas depletion timescale of  $T_{\text{dep}} = 2$  Myr (model  $A_3$ ). In the latter case, fewer asteroids retain their original orbits. The eccentricity damping occurs over a longer period of time, resulting in more extensive orbital decay from the asteroids’ main belt toward the terrestrial planet formation region before the gas disk has been depleted. This result indicates that if the dispersion time of the gas disk is sufficiently long, planetesimal clearing by the SSRs can still be effective even in the limit that the gas giant’s initial

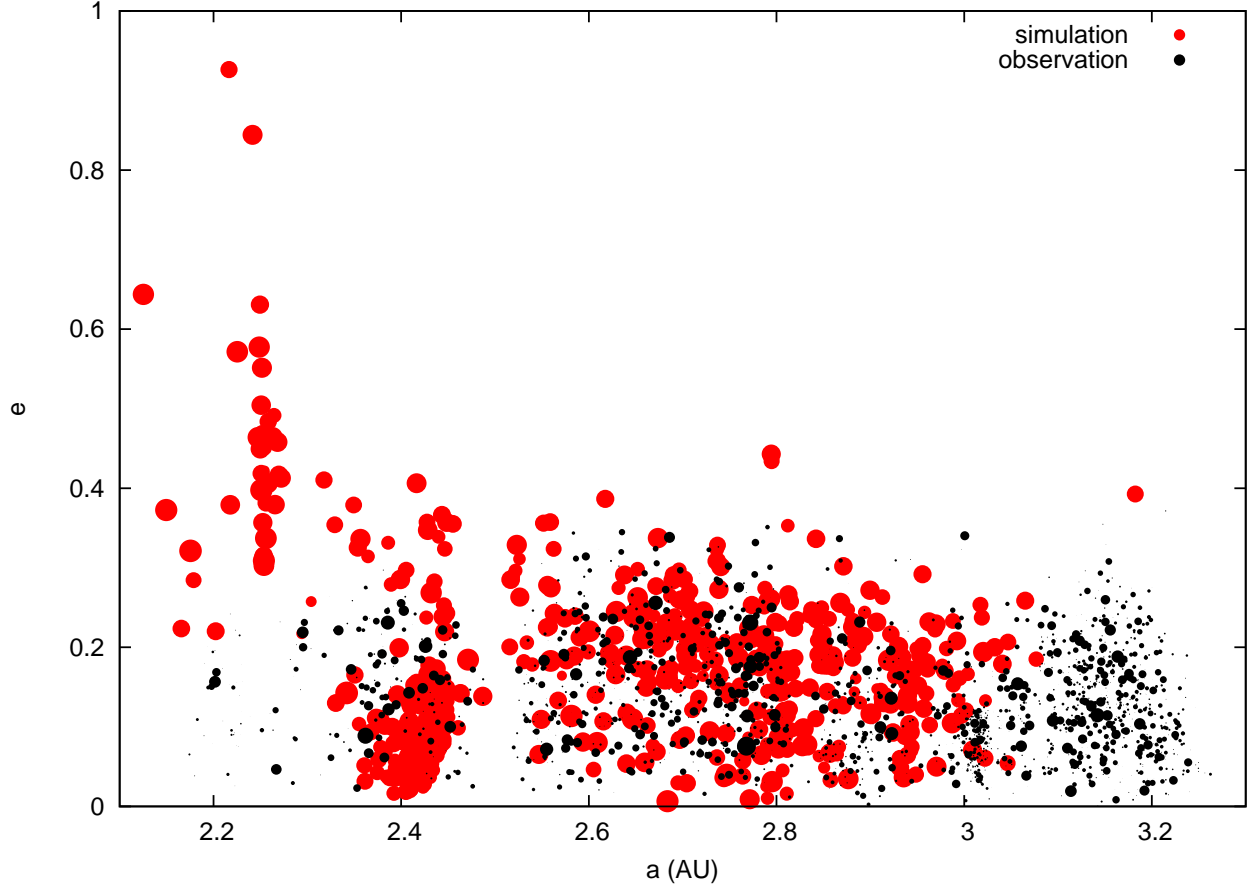


**Figure 7.** Eccentricity of the residual planetesimals (red dots) in the main belt ( $\sim 2.1 - 3.3$  AU) as a function of planetesimal semimajor axis at time  $t = 10 T_{\text{dep}}$ , for the default model  $A_1$ . The semimajor axes and eccentricities of known asteroids are plotted with black dots using the orbit data from the *Minor Planet Center orbit database*. The dots' size is scaled logarithmically to the planetesimals' radius. The labeled dots in the upper right corner correspond to  $r_p = 100$  km.

angular momentum deficit is small.

The comparison of the residual planetesimals' eccentricity distribution between models  $A_1$ ,  $A_2$ , and  $A_3$  is shown in Figure 11. For model  $A_2$ , due to the large scale height, more super-1000 km-size planetesimals remain in the main belt region, while for model  $A_3$ , fewer are left. Their eccentricity distribution (blue dots and red dots), however, is similar to that of the default model  $A_1$ , though the larger planetesimals' (with  $r_p \sim 1000$  km) eccentricities are clearly larger in model  $A_2$  than those in model  $A_1$ , just like the observed eccentricity-period distribution of known asteroids (black dots). The eccentricities of smaller planetesimals in these models have comparable dispersions and average values.

#### 4.4.2. Dependence on the gas giants

The initial eccentricity of Jupiter ( $e_J$ ) does not influence the propagation of the sweeping SRs. However,  $e_J$  does determine the angular momentum deficit of the entire system and therefore the strength of the SRs. In order to study the effect of Jupiter's eccentricity, we compare in Figure 12 the results of the default model  $A_1$  ( $e_J = 0.05$ ) and that of a system with a lower angular momentum deficit,  $e_J = 0.03$  (model  $A_4$ ). Note that for the latter model the orbital excitation due to Jupiter's SR is weakened, and therefore a larger fraction of the planetesimals are expected to retain their original orbits. The less efficient sweeping SRs tend to preferentially preserve the smaller bodies rather than the larger Moon-size embryos. This result indicates that Jupiter's primordial eccentricity can play a substantial role in the clearing efficiency of sweeping SRs. In many known exoplanet systems, gas giant planets with  $e_J \gg 0.05$  have been found. These systems have much larger angular momentum deficits. If they attained this angular momentum deficit prior to the disk depletion, sweeping SRs may have played an important role in clearing the residual planetesimals and in inducing the formation of wide dust-free gaps in some debris disks (Su et al. 2013).

The eccentricity distribution of the residual planetesimals is shown in Figure 13. We compare models  $A_1$  and  $A_4$ , and find that for the smaller  $e_J$  it is less likely for the residual planetesimals to obtain large eccentricities ( $e > 0.6$ ) due to the small angular momentum deficit of the system. However, their average values of the orbital eccentricities are similar.



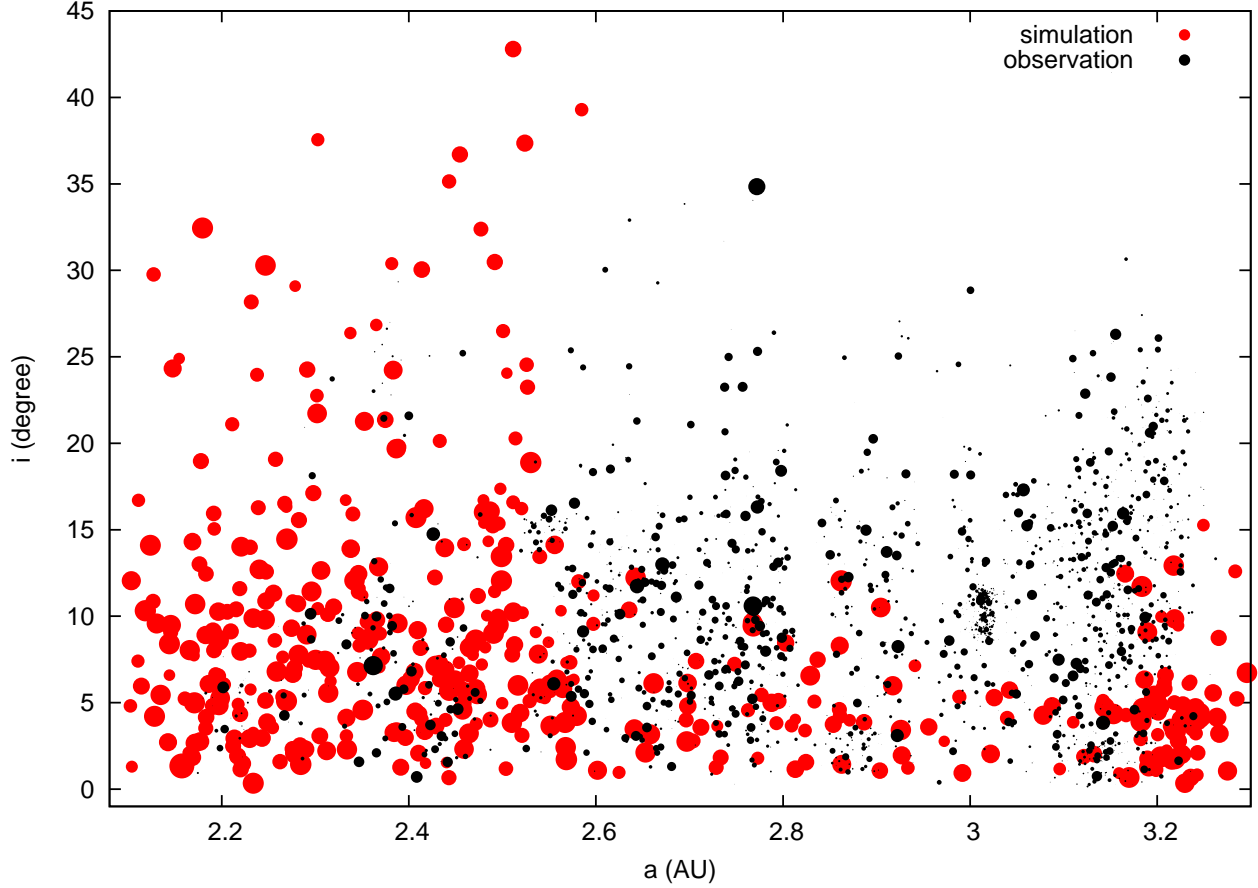


**Figure 8.** Inclination of the residual planetesimals (red dots) in the main belt ( $\sim 2.1 - 3.3$  AU) as a function of planetesimal semimajor axis at the end of simulation. The semimajor axes and inclinations of known asteroids are plotted with black dots using the orbit data from the *Minor Planet Center orbit database*. The dot sizes is scaled logarithmically to the planetesimals' radius. The labeled dots in the upper right corner correspond to  $r_p = 100$  km.

In all the models above, we took into consideration perturbation from two gas giants, Jupiter and Saturn. They are the dominant contributors to the  $\nu_5$  and  $\nu_6$  SRs, respectively. However, due to their mass difference, Jupiter's SR is generally regarded as the most powerful perturber on asteroids' dynamical evolution. In order to isolate the contribution from the  $\nu_5$  SR, we consider an idealized model  $A_5$  in which only Jupiter's perturbation is included. In Figure 14, the results of model  $A_5$  are compared with those generated with the default model ( $A_1$ ). These results show that the  $\nu_5$  SSR alone is more effective in clearing the main belt region and inducing the size selection for the residual planetesimals. In the absence of Saturn, the angular momentum deficit of Jupiter's orbit is preserved. Consequently,  $e_J$  preserves its initial value rather than modulating on a secular time scale (due to the perturbation on Jupiter by Saturn). Therefore, a larger fraction of the initial population of asteroids is cleared out in model  $A_5$  than in model  $A_1$ .

We now consider the possibility that the orbits of Jupiter and Saturn may have evolved after the phase of gas depletion. This possibility has been suggested by Gomes et al. (2005) in the Nice model for the late heavy bombardment (LHB). This scenario is based on the assumption that Jupiter and Saturn were closer to each other and their orbits evolved into their present-day configuration as they scattered and cleared away residual planetesimals in the outer solar system (Fernandez & Ip 1984). This hypothesis provides a natural explanation for the origin of MMR between Neptune and some Kuiper belt objects, including Pluto (Malhotra 1993). However, there are alternative models based on the assumption that Pluto and several Kuiper Belt objects were captured into Neptune's MMRs as a consequence of Neptune's outward migration induced by its tidal interaction with the residual gas in the outer regions of the solar nebula (Ida et al. 2000). Similar mechanisms have been proposed to account for several resonant extrasolar planetary systems (Lee & Peale 2002). Such a scenario would not require extensive post-formation migration for Saturn. In view of these possibilities, we consider several variations of our default model. In models  $A_6$ ,  $A_7$ ,  $A_8$ , and  $A_9$ , we assume Saturn's semimajor axis, at the epoch of nebula depletion, to be 8.6 AU, 9.0 AU, 9.3 AU, and 8.1 AU, respectively. Without the loss of generality, we set Jupiter's semimajor axis to be 5.2 AU.

The secular interaction between Jupiter and Saturn modifies their precession frequencies due to the disk potential

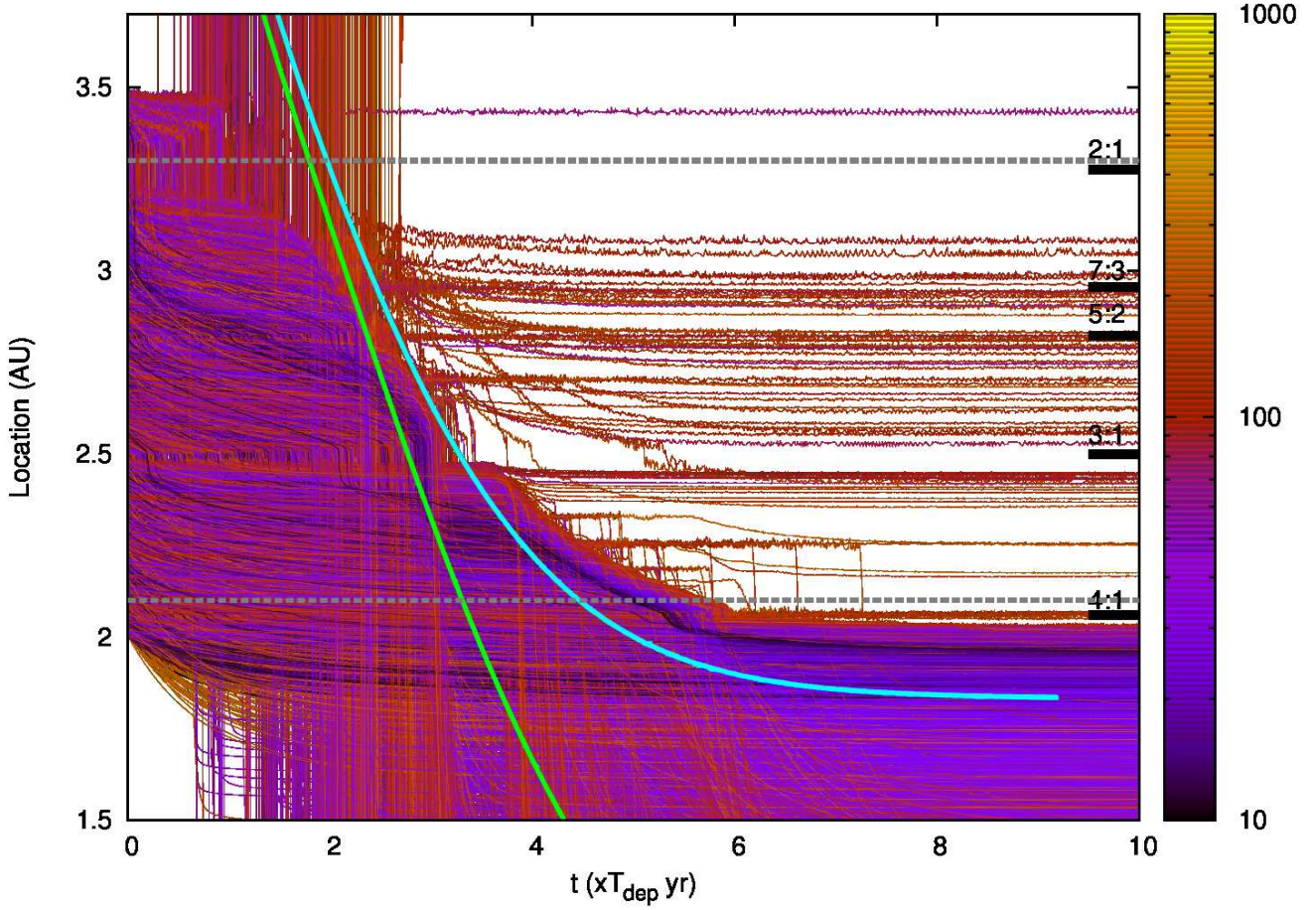


**Figure 9.** Evolution of the semimajor axes within  $10 T_{\text{dep}}$ . The sizes of the asteroids are indicated with different colors, ranging from black (10 km) to yellow (1000 km). The green and light-blue curves refer to the analytical  $\nu_5$  and  $\nu_6$ , respectively. The gray dashed lines indicate the extent of the present-day main belt.

and detunes their contribution to the  $\nu_5$  and  $\nu_6$  SRs on the residual planetesimals. The intensity of this interaction would be enhanced if they would have had a smaller  $a_S - a_J$  in the past. In such a limit, the  $\nu_5$  and  $\nu_6$  SRs would be less effective in exciting the planetesimals' eccentricities. A closer initial separation between Jupiter and Saturn also would reduce SRs' sweeping speed and causes the SRs to be stalled at larger  $a$  value during the epoch of nebula depletion.

Since  $M_J \gg M_S$ , modification of the  $\nu_5$  SSR in models  $A_6 - A_9$  from model  $A_1$  is relatively limited such that it is still effective in clearing out a large fraction of the initial planetesimal population. However, the impact of the  $\nu_6$  SSR depends more sensitively on  $a_S - a_J$  (Fig. 15). For example, in model  $A_6$  (represented by red dots), the  $\nu_6$  SR is stalled at  $\sim 2.6$  AU, and a significant fraction ( $\sim 40\%$  in total mass) of the initial planetesimal population (Fig. 17), over a wide size range, is retained interior to  $\sim 2.5$  AU. Some of these planetesimals were initially located in the region between the  $\nu_5$  and  $\nu_6$  SRs at the onset of disk depletion. Due to the stalling of the  $\nu_6$  SR, a similar population ( $\sim 20\%$  in total mass) of residual planetesimals is retained inside  $\sim 2.2$  AU in model  $A_7$  (represented by green dots). In model  $A_8$ , the  $\nu_6$  SR is stalled inside 2 AU and most planetesimals are cleared out of the main belt region. Only a small fraction (comparable to that of the default model  $A_1$ ) of the initial planetesimals within a selected size range (50 – 1000 km) is retained (see 'preferable size range' in Figure 15) in the classical main belt region ( $\sim 2.1 - 3.3$  AU).

When the semimajor axis of Saturn is reduced from 8.6 AU (model  $A_6$ ) to 8.1 AU (model  $A_9$ ), the influence of the 2:1 mean motion resonance between Jupiter and Saturn can no longer be neglected. The secular precessions of both Jupiter and Saturn are significantly altered, especially when they are near the 2:1 MMR location at  $\sim 8.25$  AU (Malhotra 1989; Murray & Dermott 1999; Agnor & Lin 2012). In model  $A_9$ , the propagation of the  $\nu_6$  SR is stalled outside  $\sim 3.35$  AU, while the  $\nu_5$  SR still sweeps through the main belt region, albeit at a slower pace. The dynamical evolution of the planetesimals is similar to that in model  $A_5$  (with Jupiter only). The stagnation of the  $\nu_6$  SR prevents the accumulation of a significant population of residual planetesimals in the main belt region. The fraction of the initial population of planetesimals ( $10^{-4}$  in mass) retained in model  $A_9$  is an order of magnitude smaller than that of the

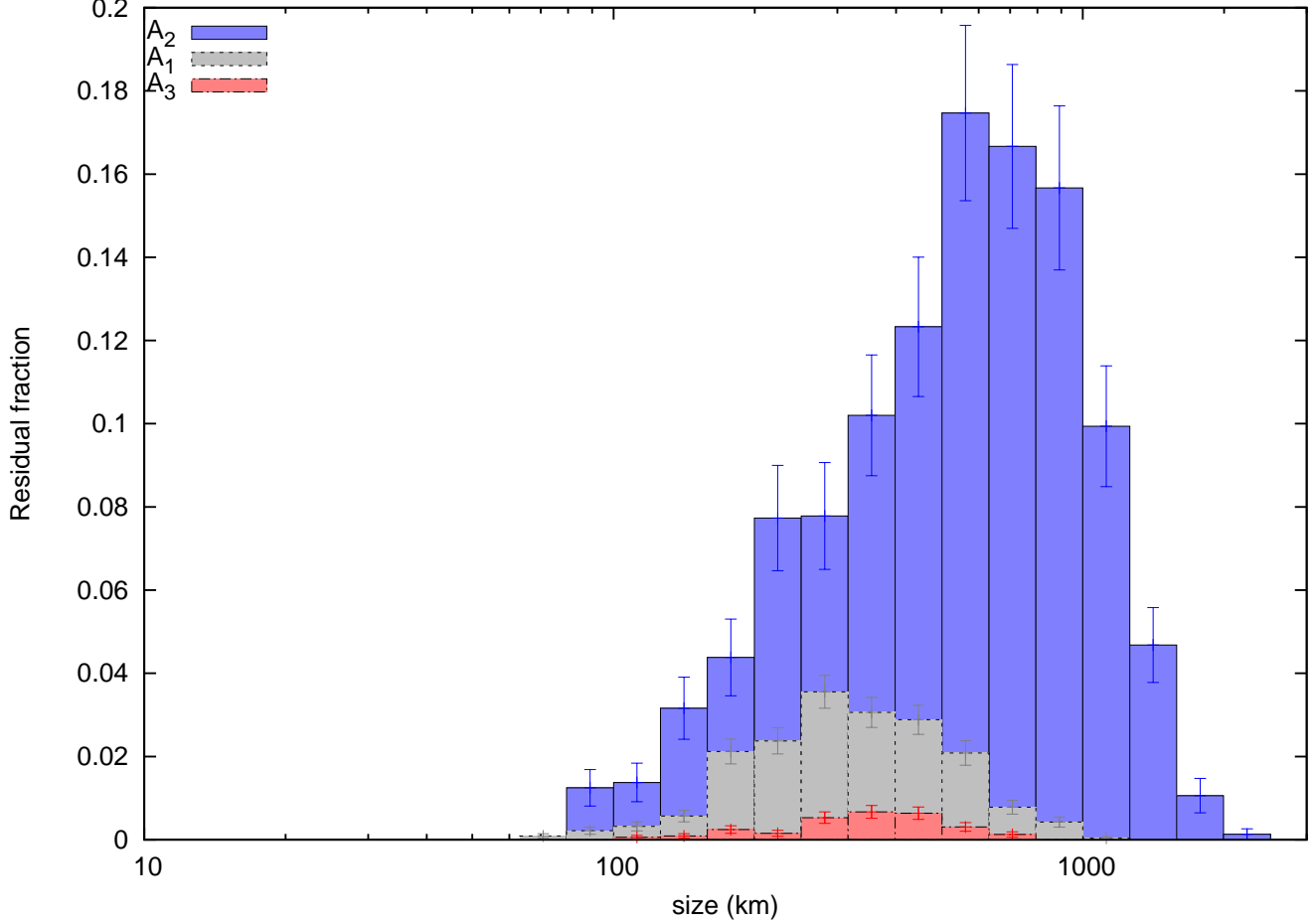


**Figure 10.** Model dependence for disk scale heights  $h_0$  and the gas depletion timescale  $T_{\text{dep}}$ . The gray histogram shows the results for the default model  $A_1$  with  $h_0 = 0.025$ ,  $T_{\text{dep}} = 1$  Myr. The blue histogram shows the results for model  $A_2$  with  $h_0 = 0.05$ ,  $T_{\text{dep}} = 1$  Myr. The red histogram represents the results for the model  $A_3$  ( $h_0 = 0.025$ ,  $T_{\text{dep}} = 2$  Myr)

default model  $A_1$ . The total mass of the residual planetesimals in this case is also smaller than that of the present-day asteroid belt. The residual planetesimals would not be able to provide a reservoir of asteroids to accommodate the LHB induced by Saturn’s subsequent passage through Jupiter’s 2:1 MMR (in accordance with the Nice model) unless many more residual planetesimals may be retained with a much shorter ( $\ll 1$  Myr) nebula depletion time scale (Fig. 16). These results indicate that during the epoch of disk depletion, efficient clearing of residual intermediate-size planetesimals requires either the separation of Jupiter and Saturn ( $a_s - a_J$ ) to be within  $\leq 0.5$  AU of its present-day value (i.e., the migration of both gas giants after the gas depletion was limited) or that they were located near their 2:1 MMR. For the latter possibility, the clearing of residual planetesimals may be overly efficient.

In models  $A_6$  and  $A_7$ , Saturn still has to undergo further orbital migration to its present-day kinematic configuration after the gas depletion phase. During this late phase of orbital evolution, the eccentricities of the residual planetesimals are excited in the absence of both hydrodynamic and tidal damping. Their semimajor axes are not affected by the SSRs. Nevertheless, their enhanced eccentricity may lead to orbit crossing with the terrestrial planets and subsequent dynamical instabilities. In order to consider this possibility, we simulated the dynamical evolution of the residual planetesimals (mainly located between 2.1 AU and 2.4 AU, size of 10 to 1000 km) in model  $A_6$  with an outward migration of Saturn over two different time scales (1 and 0.5 Myr). In the left and right panels of Figure 18, we plot the asymptotic eccentricity for different-size planetesimals in the main belt region. During Saturn’s migration,  $\nu_6$  sweeps from  $\sim 2.6$  to  $< 2.1$  AU. Planetesimals retained in this region after the nebula depletion are further excited. In the absence of any effective eccentricity damping, most of the residual planetesimals retain somewhat larger eccentricities. And the maximum amplitude of those eccentricities is correlated with the migration time scale of Saturn. Protracted migration (on a time scale  $> 1$  Myr) generally excites the eccentricity of the residual planetesimals above that of the observed asteroids ( $e < 0.3$ ). The eccentricity of some residual planetesimals may be sufficiently large for them to cross the orbits of the terrestrial planets and become dynamically unstable. In a gas-free environment, size selection among the retained planetesimals is no longer possible.

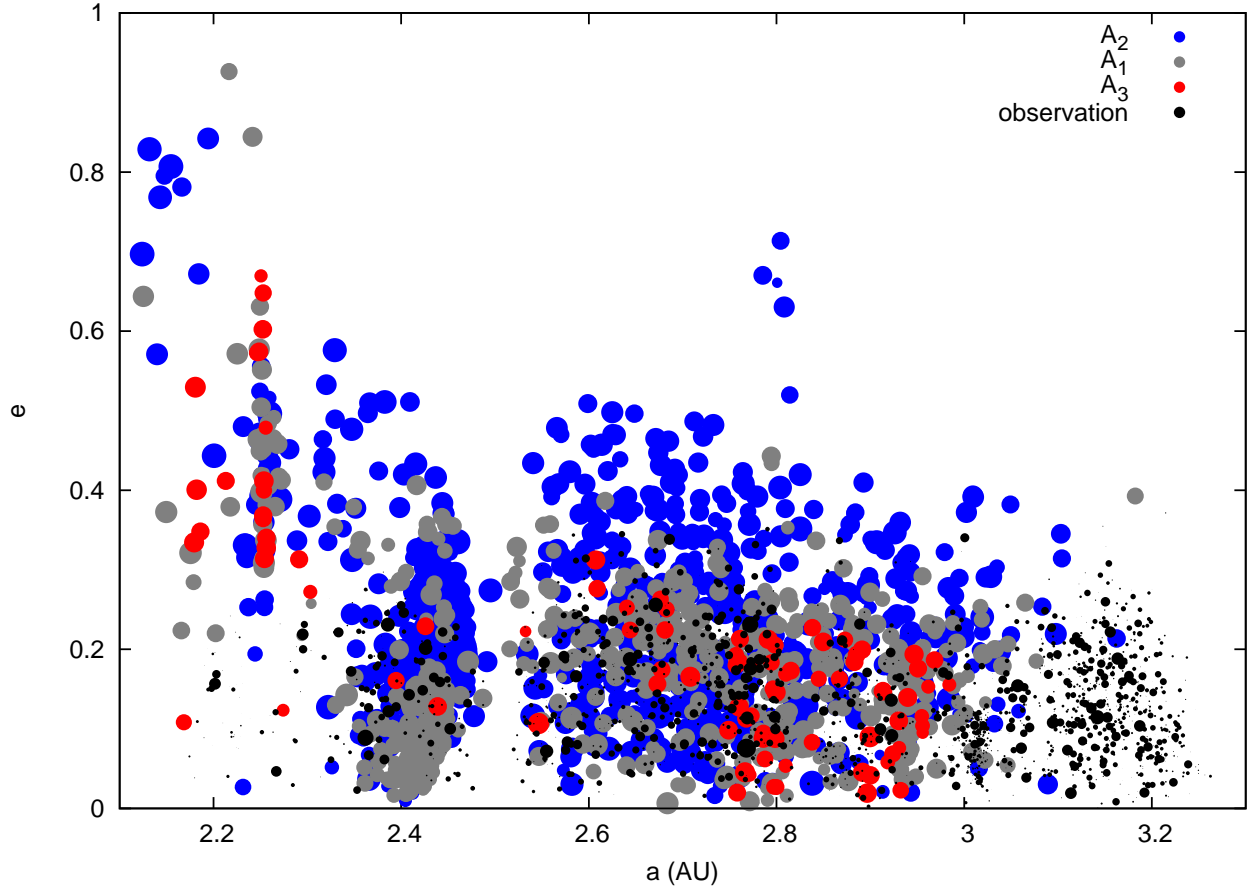


**Figure 11.** Eccentricity vs. semimajor axis and size of the residual planetesimals. The gray dots show the result of default model  $A_1$ , while the red dots and blue dots are the results for models  $A_3$  and  $A_2$ , respectively. Black dots are observed data from the *Minor Planet Center orbit database*. The dots’ size is scaled logarithmically to the planetesimals’ radius. The labeled dots on the upper right corner correspond to  $r_p = 100$  km.

In models  $A_6 - A_9$ , we have not considered the possibility that Jupiter may have migrated as extensively as hypothesized in the “grand-tack” model (Walsh et al. 2011). In such a scenario, most of the planetesimals formed in the main belt region would be scattered into the terrestrial planet zone and the  $\nu_5$  and  $\nu_6$  SSRs would have little impact on the essentially empty main belt region during the depletion of the disk gas. The migration paths of multiple planets depend sensitively on the initial conditions and boundary conditions of the solar nebula, as well as the time lapse between Jupiter’s formation and Saturn’s formation and their gas accretion rates. In light of these uncertainties, we consider here an alternative possibility under the assumption that Jupiter and Saturn’s migration was limited in range. Our results confirm that  $\nu_5$  and  $\nu_6$  SSRs alone can lead to the extensive inward migration of the planetesimals from the main belt region to the terrestrial planet zone. They also show that the intermediate-size planetesimals are preferentially retained, regardless of the initial value of  $a_S$ .

## 5. SUMMARY AND DISCUSSION

We have constructed a sweeping SR model to explain the observed properties of the main asteroid belt without the necessity of introducing additional assumptions about the origin and evolution of planetesimals. Using this model, we are able to reproduce (i) the apparent mass deficit of the present-day main asteroid belt (Fig. 6; see also Morbidelli et al. 2009), (ii) the observed SFD of the asteroids in the main belt (Fig. 5), (iii) the semimajor axis and eccentricity distributions of residual planetesimals (Fig. 7), and (iv) substantial radial mixing (Fig. 9).

Some of these issues have already been considered previously by several other investigators, especially those associated with the Nice school. In this summary and discussion section, we make several detailed comparisons between our results and those obtained with other promising models. We highlight here some tension between various models and suggest that our sweeping SR hypothesis offers a viable alternative, at least in the context of asteroids’ size-frequency and spacial distributions.

### 5.1. Comparison with the “ab initio large” model for the asteroids’ SFD

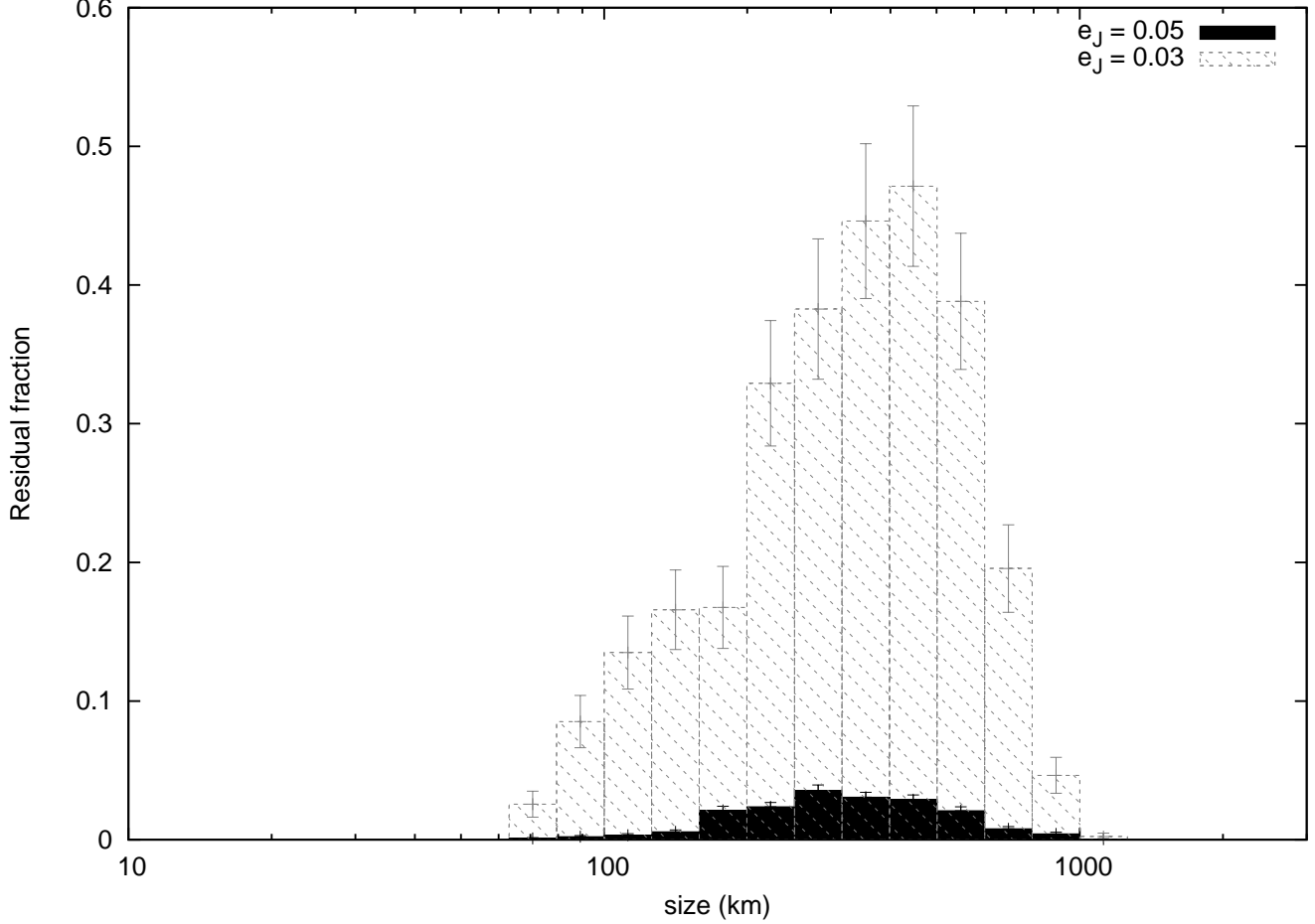


**Figure 12.** The  $e_J$  dependence of the retention efficiency and asymptotic SFD of asteroids. The black histogram represents the results for the default model  $A_1$  ( $e_J = 0.05$ ) and the hatched histogram is for  $e_J = 0.03$  (model  $A_4$ ).

We have seen in this paper that planetesimal eccentricities can be excited through the exchange of angular momentum with Jupiter and Saturn through their MMRs and SRs, and that eccentricity damping leads to energy dissipation and the orbital decay of planetesimals. In our models, we assume that the surface density of the nebula decreases everywhere with a radius-independent depletion factor. We show that even after the disk gas is sufficiently depleted to enable the  $\nu_{5,6}$  SRs to sweep through the main belt region, eccentricity damping continues to be effective in causing some planetesimals to undergo orbital decay. This eccentricity damping process is particularly effective for the small planetesimals, due to the hydrodynamic drag, and for the large embryos, due to their tidal interaction with gas in the solar nebula. The competition between these two damping mechanisms leads to planetesimals' size-dependent orbital decay rates. The similarity between the size distributions of the residual planetesimals and the observed SFD provides an alternative scenario for the origin of the asteroids. In contrast, [Morbidelli et al. \(2009\)](#) propose an “*ab initio* large” model that requires the minimum size of the primary planetesimals,  $\sim 100$  km in diameter, to reproduce the observed “bump” feature in the present-day SFD of the asteroids; however, a new planetesimal formation scenario is required in this model.

### 5.2. Comparison with previous models for the planetesimal removal from the main belt region

In a related analysis, [O’Brien et al. \(2007\)](#) showed that the SR sweeping can neither excite the eccentricity nor efficiently clear the residual planetesimals. The main difference between their and our results is mainly due to their neglect of any damping of the planetesimals' excited eccentricities. They justified this approximation with a scenario in which the solar nebula may have been cleared outward from its center. They also considered the SR sweeping effect with a radius-independent depletion model, in which there would be a non-negligible amount of residual gas in the main belt region. However, they did not explicitly compute the contribution of this residual gas on the eccentricity damping for the most vulnerable planetesimals in the main belt region.

For the orbital parameters of Jupiter and Saturn, [O’Brien et al. \(2007\)](#) adopted (1) a Nice model with negligible eccentricity ([Gomes et al. 2005](#)) and (2) their present-day values. With nearly circular orbits, the amount of angular



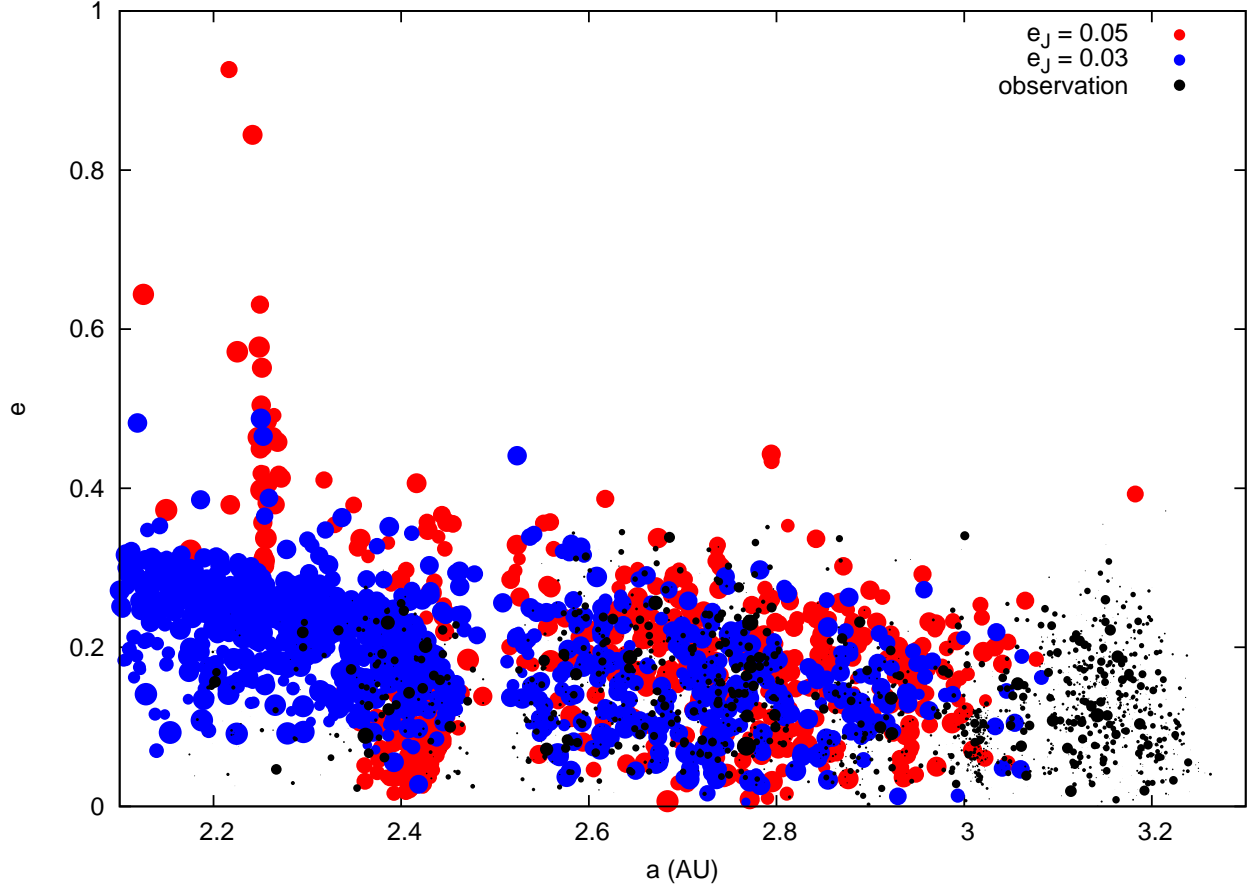


**Figure 13.** Eccentricity as a function of  $(a, r_p)$ , for the residual planetesimals, for different eccentricities of Jupiter. The red dots show the results for  $e_J = 0.05$ , and the blue dots are the results for  $e_J = 0.03$ . Black dots are observed data from the *Minor Planet Center orbit database*. The dots' size is scale logarithmically to the planetesimals' radius. The labeled dots on the upper right corner correspond to  $r_p = 100$  km.

momentum Jupiter and Saturn can receive would be limited. They found that the excitation of planetesimals' eccentricities to the present values of the asteroids would require a slow propagation of the SRs with an implied gas-depletion time scale  $> 10$  Myr. With the present-day eccentricities of Jupiter and Saturn, planetesimal eccentricities can be adequately excited within a few megayears. However, since the SRs do not directly lead to energy transfer, they found that most planetesimals' semimajor axes would not be affected by the passage of Jupiter's and Saturn's SRs.

Based on the discussions in §2, we adopted in our default model  $A_1$ , an angular momentum deficit for the Jupiter-Saturn configuration to be 2/3 of its present-day value. Similar to the O'Brien et al. (2007) present-day model, our model  $A_1$  reproduces the observed eccentricity-semimajor-axis distribution of the residual intermediate-size planetesimals. When a quasi-equilibrium in eccentricity excitation/damping is established, Jupiter's and Saturn's MMRs and sweeping SRs relocate  $> 99\%$  of the initial planetesimals in the main zone region to regions interior to 2 AU. These contrasting conclusions on whether the sweeping SRs can remove most of the residual planetesimals from the main belt region are determined by the assumed efficiency of eccentricity damping.

### 5.3. Comparison with the Embedded-embryos model for the planetesimal eccentricity excitation

In the core accretion scenario, the formation of gas giant planets is preceded by the emergence of protoplanetary embryos with masses comparable to or larger than that of the Earth (Pollack et al. 1996; Ida & Lin 2004). These embryos are embedded among residual planetesimals in the gas-rich nebula. Wetherill (1992) suggested that the eccentricity and inclination of embryos and planetesimals in the main belt region may be excited by Jupiter's MMRs and SRs. This hypothesis was confirmed by a series of numerical simulations (Chambers 2001; Petit et al. 2001) which showed that through encounters between them, planetesimals may be cleared from the main belt region, while the more massive embryos are retained in the main belt region.

In the embedded-embryo scenario, O'Brien et al. (2007) showed that up to  $\sim 90 - 95\%$  of the residual planetesimals may be cleared over at least several megayears. Despite this remarkable reduction, the surface density of the residual planetesimals would still be an order of magnitude larger than that of the present-day asteroid population. One

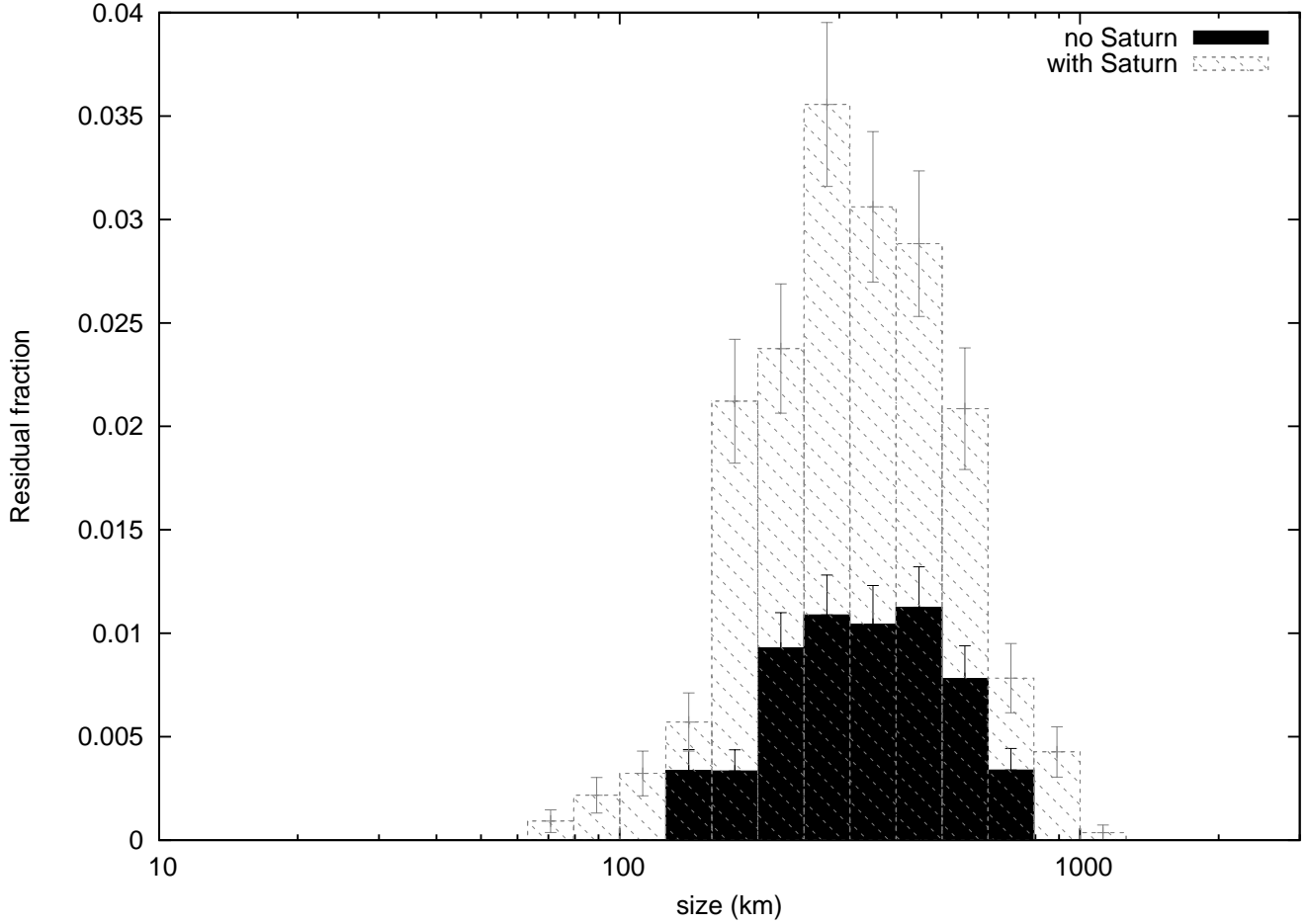


**Figure 14.** Influence of Saturn’s secular perturbation on Jupiter. The hatched histogram represents the results for the default model  $A_1$  (both Jupiter and Saturn included), and the black histogram is for model  $A_5$ , in which the contribution from Saturn is neglected.

possible scenario to make up this difference has been suggested on the basis of the Nice model for LHB. During the early stages of solar system evolution, it is likely that Saturn may have migrated outward as it scattered planetesimals in the outer solar system to even larger heliocentric distances (Fernandez & Ip 1984; Malhotra 1993). The Nice LHB model is based on the assumption that Saturn has migrated over  $\sim 2$  AU. It attributes the LHB event and the capture of Trojan asteroids to the passage of Saturn’s orbit through its 2:1 MMR with Jupiter at  $\sim 3.8$  Gyr ago. At that time, the surface density of the residual planetesimals in the main belt region may be reduced by an order of magnitude due to the clearing of the sweeping SRs (Gomes et al. 2005; Morbidelli et al. 2005; Tsiganis et al. 2005).

Our model adopts some similar assumptions to the embedded-embryo model, such as an initial planetesimal size distribution that includes the existence of relatively massive embryos. We also adopt a subset of the initial conditions assumed by the Nice model. For example, we only consider a radius-independent depletion factor (§5.1), and we adopt a modest angular momentum deficit rather than nearly circular orbits for the Jupiter-Saturn system (§5.2). With our default model  $A_1$ , we showed that as they sweep through the solar nebula, the  $\nu_5$  and  $\nu_6$  SSRs can excite planetesimals’ eccentricities. Effective hydrodynamic and tidal drag damps planetesimals’ eccentricities and induces them to undergo orbital decay. Our results suggest that most of the small asteroids and large embryos are removed from the main belt region during the first few megayears of solar system evolution.

Based on previous investigations (Heppenheimer 1980; Ward 1981; Nagasawa et al. 2000), we recognize that asteroids’ present-day inclination cannot be excited by Jupiter’s and Saturn’s secular perturbation during the nebula’s depletion because their inclination resonances do not sweep through the main belt region. We showed with the parameters of model  $A_1$ , that the mutual perturbations between planetesimals (with sizes in the range of 100 – 1000 km) and a few embryos (with sizes 1000 – 3000 km) can adequately excite the inclinations of intermediate-size planetesimals to observed values (Fig. 8). We suggest that these planetesimals are most likely to be the progenitors of the asteroids as they are preferentially retained in our model.

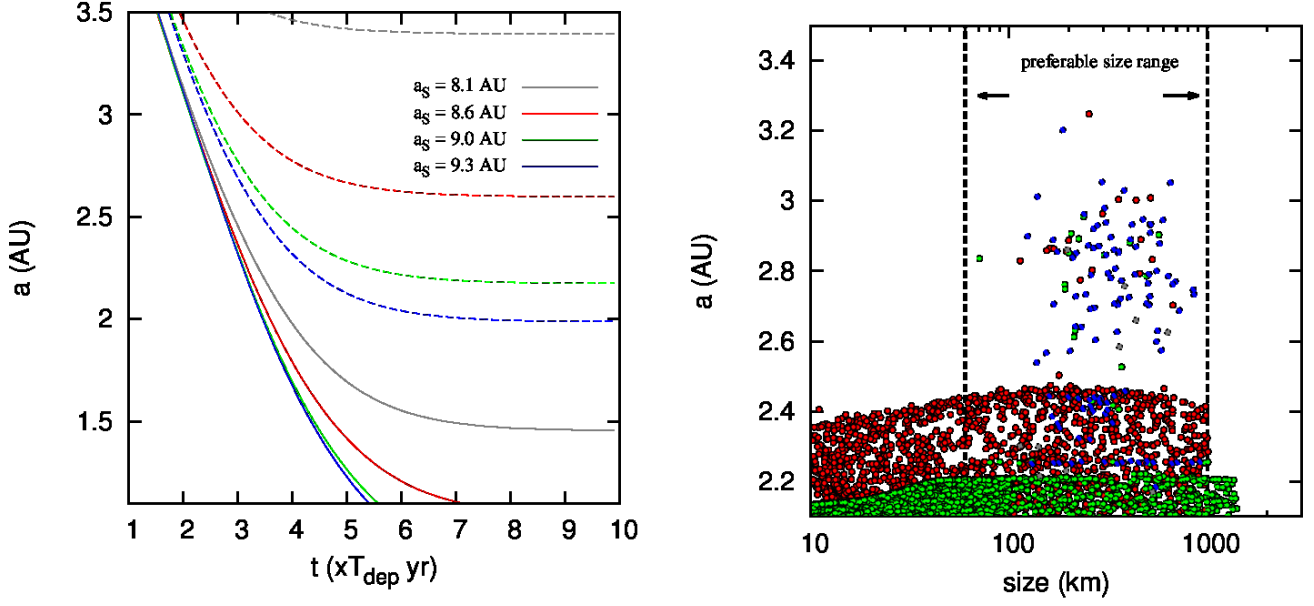


**Figure 15.** Comparison between the results for models with different Jupiter-Saturn separations. The left panel shows the sweeping paths of  $\nu_5$  (solid curves) and  $\nu_6$  (dashed curves). We adopt the present-day location of Jupiter. Colors label the cases in which the initial semimajor axis of Saturn is 8.6 AU (red: model  $A_6$ ), 9.0 AU (green: model  $A_7$ ), 9.3 AU (blue: model  $A_8$ ) and 8.1 AU (gray: model  $A_9$ ). The right panel shows the planetesimals’ locations at  $t = 10 \text{ Myr}$  as a function of size, and as a function of Saturn’s initial location (models  $A_6 - A_9$ ).

#### 5.4. Comparison with the Grand-tack model for the removal of embryos from the main belt region

An implication of the embedded-embryo scenario is that a population of relatively massive embryos needs to be retained in the main belt region as scattering agents until most of the residual planetesimals are cleared. Due to dynamical friction, the velocity dispersion of the embryos is expected to be smaller than that of the lower-mass planetesimals (Wetherill & Stewart 1989; Palmer et al. 1993). However, a protracted retention of embryos may lead to the formation of terrestrial planets in the main belt region. Hansen (2009) showed that the spacial distribution of the terrestrial planets requires their building blocks to be confined within  $\sim 2 \text{ AU}$ . A confinement mechanism has been suggested by Walsh et al. (2011). This “grand-tack” scenario is based on the assumption that due to its tidal interaction with the disk gas (in consort with Saturn), Jupiter may have migrated inward through the solar nebula and then outward over a few AU to its present-day location. During this course of this excursion, most of the planetary building blocks would be swept into the inner solar system. The probability of such an excursion is uncertain. Since Jupiter migration is driven by its tidal interaction with the disk, this process cannot occur after the depletion of the disk gas.

In the embedded-embryos scenario (O’Brien et al. 2007), the time scale for 90% planetesimal clearing by an assumed population of embedded Mars-size embryos (with a total mass of  $5M_{\oplus}$ ) is  $\sim 10 \text{ Myr}$ , which is comparable to or longer than the observed gas depletion time of  $\sim 3 - 5 \text{ Myr}$  (Hartmann 1998). The “grand-tack” scenario would make the embedded-embryos scenario obsolete if both embryos and planetesimals are appreciably cleared from the main belt region by a migrating Jupiter. The removal efficiency is independent of planetesimals’ mass and radius, and therefore it does not lead to a size selection for the retained progenitors of asteroids. Partial reduction of the embryo population would reduce the scattering centers and their efficiency in the planetesimals’ inclination excitation.

In our model, the rate of planetesimals’ orbital decay is mostly determined by the magnitude of eccentricity and

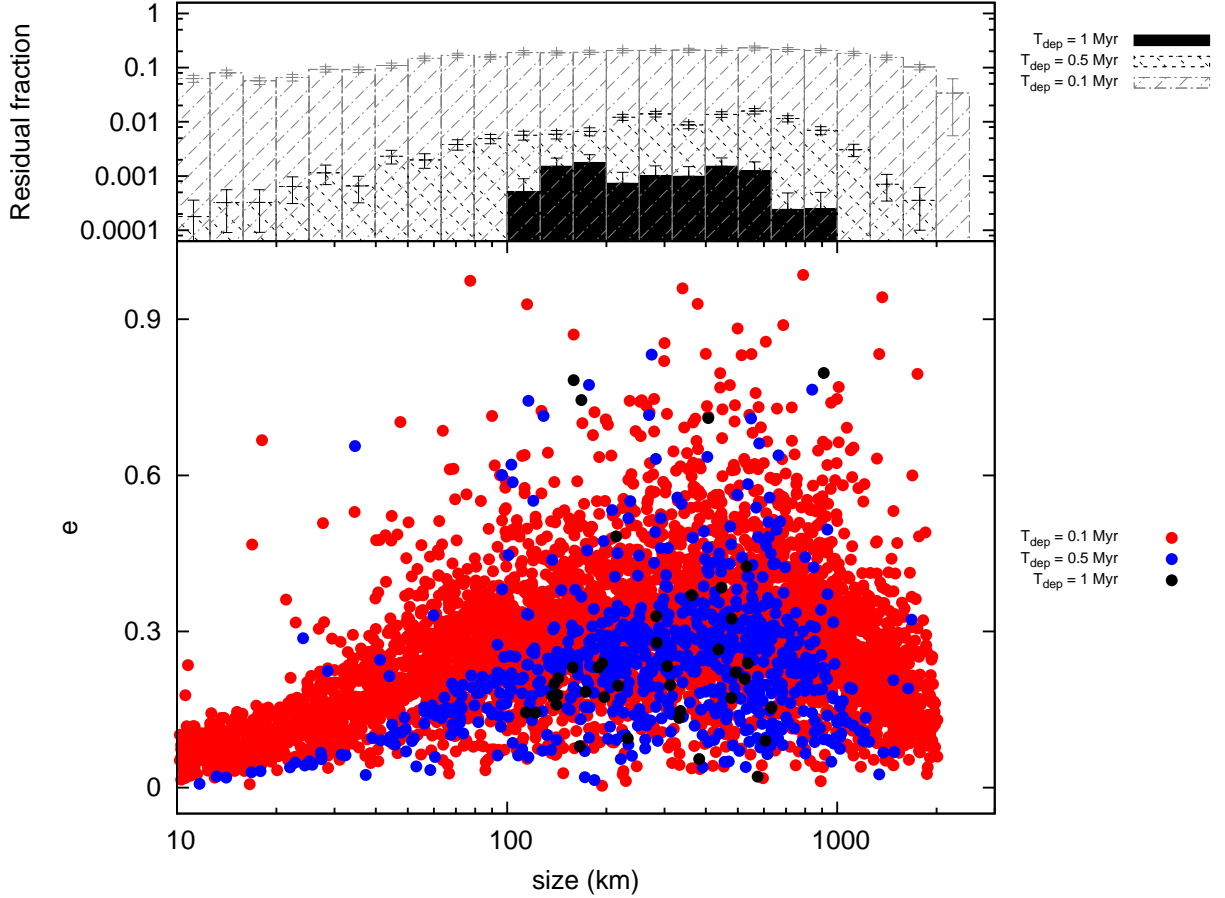


**Figure 16.** Top: Fraction of an initial population of different-size planetesimals retained in the main belt (2.1 – 3.3 AU) region in models  $A_9$  with  $T_{\text{dep}} = 1$  Myr (solid black), 0.5 Myr (short dashed), and 0.1 Myr (long dashed). Both the fraction and size range of the residual planetesimals decrease with  $T_{\text{dep}}$ . Bottom: asymptotic eccentricity of different-size residual planetesimals in models  $A_9$  with  $T_{\text{dep}} = 1$  Myr (black), 0.5 Myr (blue), and 0.1 Myr (red). The correlation between the planetesimals’ retention fraction and  $T_{\text{dep}}$  is determined by the efficiency of eccentricity damping. For relatively short  $T_{\text{dep}}$  ( $< 0.5$  Myr), a fraction of intermediate-size planetesimals have sufficiently eccentricity for them to cross the orbits of terrestrial planets and become dynamically unstable. The asymptotic eccentricity of all residual planetesimals decreases with  $T_{\text{dep}}$ .

its damping timescale. In the unperturbed regions, the velocity dispersion of small planetesimals is modest and that of large planetesimals is small. But their eccentricity is excited above  $e > 0.5$  during the passage of SRs or MMRs (Fig. 3). With relatively small damping timescale (Fig. 4), the large planetesimals (embryos) undergo orbital decay in consort with the inwardly sweeping SRs. In contrast, the eccentricity damping is less efficient for the intermediate-size planetesimals, and they are preferentially retained with eccentricities (Fig. 7) comparable to that ( $e \sim 0.2$ ) of most asteroids with radius larger than 50 km (Knezevic & Milani 2003).

The time scales for  $\nu_5$  to propagate to the present semimajor axes of Mars and Earth are  $4T_{\text{dep}}$  and  $10T_{\text{dep}}$ , or  $\sim 12$  and 30 Myr, for the observationally inferred value  $T_{\text{dep}} \sim 3$  Myr. The passage of the  $\nu_5$  SR leads to eccentricity excitation, which promotes orbit crossing and physical collisions among the inwardly migrating embryos. Nagasawa et al. (2005) and Thommes et al. (2008) proposed a “dynamical shake-up” model to account for the formation time scale of terrestrial planets as inferred from cosmochemical data (Kleine et al. 2009) and their modest eccentricities.

##### 5.5. Comparison with previous models on the initial eccentricity and semimajor axes of the Jupiter-Saturn system

Throughout this paper, we have emphasized that efficient damping of excited eccentricity is essential for the clearing of planetesimals. O’Brien et al. (2007) have already shown that with nearly circular orbits, Jupiter and Saturn SRs cannot significantly excite the planetesimals’ eccentricity over the observed gas depletion time scale of 3 – 5 Myr. In model  $A_1$ , we show that a significant fraction of Jupiter and Saturn present-day angular momentum deficit is required for their SRs to excite the planetesimals’ eccentricity to an adequate level for the depletion of the initial planetesimals in the main belt region to the current asteroid population. We also simulated model  $A_4$  with a reduced amount of angular momentum deficit for the Jupiter and Saturn system. A comparison of the results generated from models

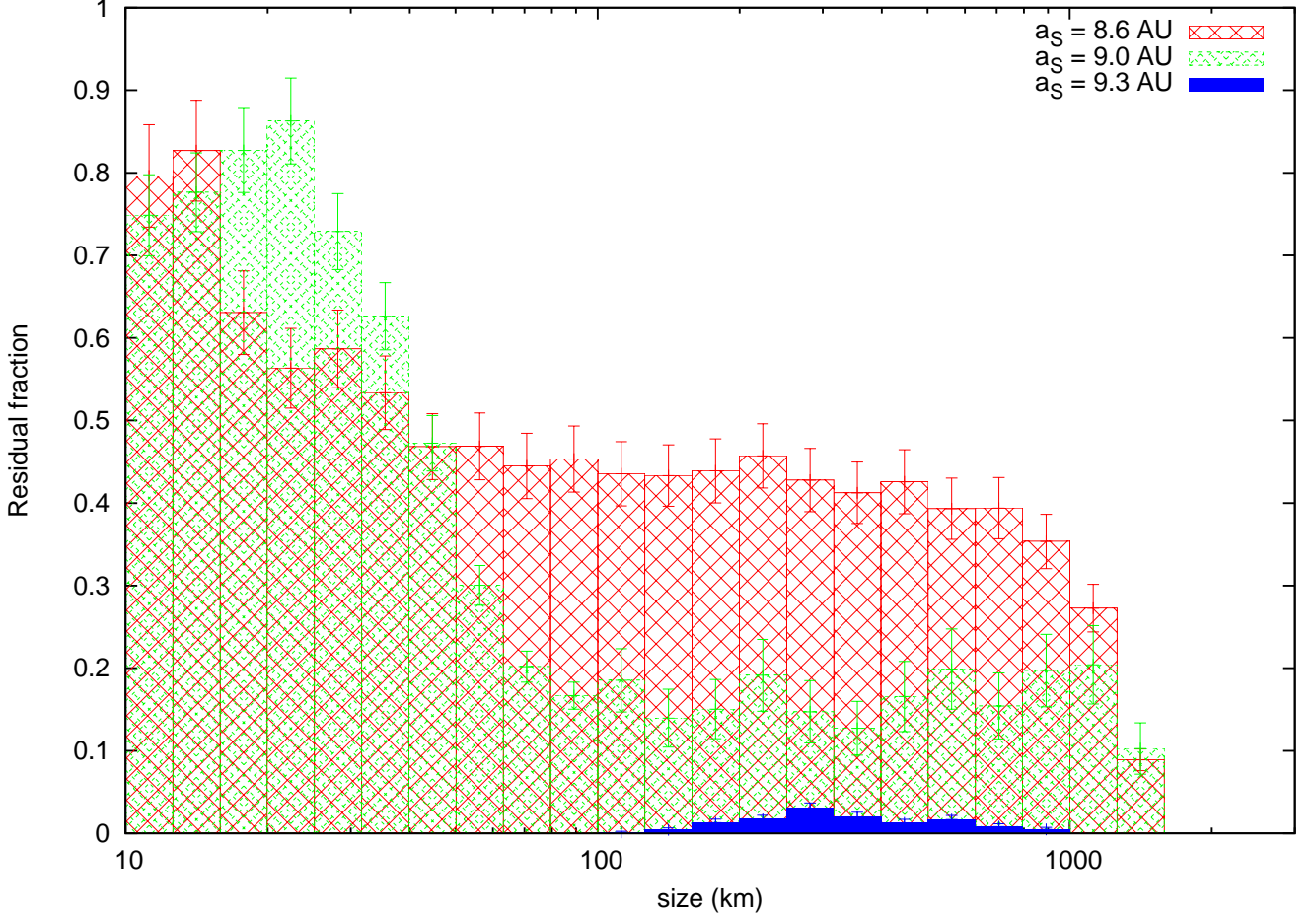


**Figure 17.** Fraction of an initial population of different-size planetesimals retained in the main belt (2.1 – 3.3 AU) region in models  $A_6$  (red),  $A_7$  (green), and  $A_8$  (blue). These results indicate that a much larger fraction of residual planetesimals of all sizes may be retained near the inner boundary of the main belt due to the stalling of the  $\nu_6$  SR if Saturn was located at  $a_s = 8.6$  AU or 9.0 AU at the epoch of nebula depletion.

$A_1$  and  $A_4$  (Fig. 12) confirms the expectation that the efficiency of eccentricity excitation and planetesimal clearing increases with  $e_J$ .

Several previous models have suggested that Saturn may have migrated outward over some significant distances. For example, the Nice model has attributed the LHB to the passage of Saturn through Jupiter’s 2:1 MMR which is currently located at 8.18 AU. In model  $A_6 - A_9$ , we consider the possibility of a closer initial Jupiter-Saturn separation. The results of these simulations show that both the MMRs and SSRs can efficiently clear both small and large planetesimals while retaining intermediate-size planetesimals in the main belt region if, during the epoch of disk depletion, Jupiter and Saturn were sufficiently close to their present-day location (models  $A_1$  and  $A_8$ ). If Jupiter and Saturn were close to each other’s 2:1 MMR (model  $A_9$ ) during the epoch of nebula depletion,  $< 10^{-4}$  in mass of the initial population of planetesimals may be retained. This total mass is less than that in the asteroid belt. More mass may be retained to accommodate a sufficiently larger reservoir of residual planetesimals for the LHB if the nebula depletion time scale is substantially less than 1 Myr. These results place some constraints but do not eliminate the possibility that Saturn may have undergone extensive outward migration. After the nebula depletion, passage of Saturn through its 2:1 MMR with Jupiter, as envisioned in the Nice model, may cause the excitation of terrestrial planets’ as well as asteroids’ eccentricity beyond their present-day values (Agnor & Lin 2012).

If Saturn was initially located between Jupiter’s 2:1 MMR and its present-day location (e.g., with a semimajor axis  $\sim 10 - 15\%$  smaller than its value today), the sweeping path of  $\nu_6$  would be stalled outside the inner boundary of the main belt region. Models  $A_6$  and  $A_7$  show that a population of planetesimals of all sizes would be retained around the provisional location of the  $\nu_6$  SR (Fig. 15). When Saturn eventually migrates to its present-day location after the disk gas is depleted, the eccentricity of the residual planetesimals would be excited as the  $\nu_6$  SR sweeps past them, but they would not undergo orbital decay without any eccentricity damping. Although the orbits of some highly eccentric planetesimals may be destabilized by the terrestrial planets’ perturbation, a large fraction of the residual planetesimals



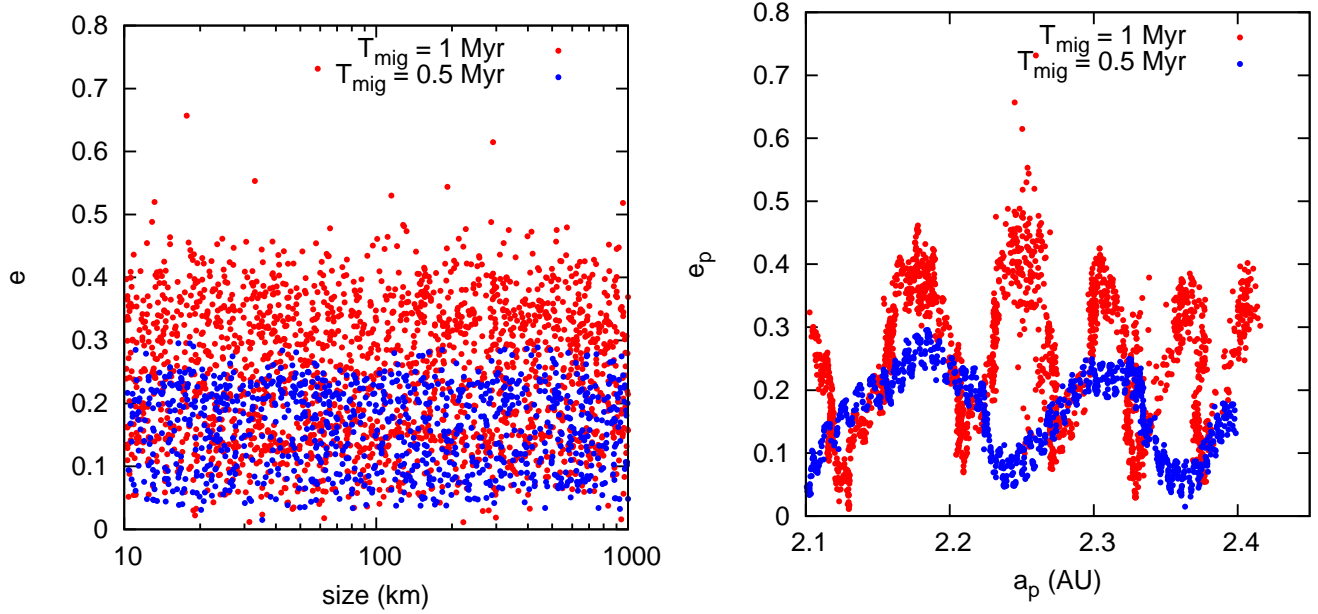


**Figure 18.** Kinematic properties of the residual planetesimals resulting from Saturn’s migration after gas in the nebula is depleted. The semimajor axis and eccentricity distributions of the planetesimals are obtained from model  $A_6$ . Saturn is assumed to have migrated outward from 8.6 AU to its present-day orbit over a time scale  $T_{\text{mig}} = 0.5 \text{ Myr}$  (blue dots) and 1 Myr (red dots). Left panel: the asymptotic eccentricity of residual planetesimals in the main belt region. Right panel: The semimajor-axis-eccentricity distribution of the residual planetesimals. The planetesimals’ semimajor axes do not change significantly during Saturn’s outward migration, but their orbits can become dynamically unstable due to the perturbations by both the terrestrial planets and the ice giants.

of all sizes would be retained within the main belt region.

### 5.6. Future investigations

We mainly focus on the dynamical depletion of asteroids in the main belt. During this process, the transitional disk and the gas giants are responsible for the gravitational perturbations on the asteroids. In this paper, we assumed a global depletion factor for the solar nebula. Photoevaporation and disk winds may lead to preferential locations for mass loss. Under some circumstances, inside-out clearing of the disk may promote planetesimals’ inclination excitation. In addition, the disk also provides a damping force that affects the embedded planetesimals. In most models, we have not included the mutual interaction between planetesimals. Although this assumption is adequate for the determination of the planetesimals’ eccentricity and semimajor axis evolution, this effect needs to be included (as in the modified default model) to enable us to account for the excitation of planetesimals’ inclination by embedded embryos (Fig. 8). We have also neglected collisions between asteroids and their subsequent fragmentation. Quantitative estimates suggest that the collision time scale is  $> 4.6 \text{ Gyr}$  for asteroids larger than  $\sim 50 - 100 \text{ km}$  such that the transitions of SFD power index in this size range have not evolved significantly since the formation of the solar system. Nevertheless, collisions and fragmentations may have significantly modified the small-size range of the observed SFD. Follow-up investigations on planetesimal-embryo interaction and on fragmentation process are warranted.

Our model supports the SSR model as the process that lead to the asteroids’ present-day SFD. Since all planetary systems originally form in circumstellar gas disks that evolve and ultimately dissipate, this model, as studied in this paper, can be applied to construct models that account for the kinematic structure of a wide range of observed extrasolar planetary systems. Such analysis will provide useful clues and place important constraints on protoplanets’

birth environment and their post-formation dynamical evolution (Zheng, X.C. et al, in preparation).

## ACKNOWLEDGMENTS

We wish to thank the anonymous reference for carefully reading the manuscript and providing useful feedback that helped to improve the paper. This work was supported in part by a UC/Lab Fee grant. We thank Shude Mao, Qingzhu Yin, Makiko Nagasawa, Shigeru Ida, and Munan Gong for useful and stimulating conversations. M.B.N.K. was supported by the Peter and Patricia Gruber Foundation through the PPGF fellowship, by the Peking University One Hundred Talent Fund (985), and by the National Natural Science Foundation of China (grants 11010237, 11050110414, 11173004, and 11573004). This publication was made possible through the support of a grant from the John Templeton Foundation and National Astronomical Observatories of the Chinese Academy of Sciences.

## REFERENCES

- Aarseth, S. J., Lin, D. N. C., & Palmer, P. L. 1993, *ApJ*, 403, 351  
Aarseth, S. J. 2003, *Gravitational N-Body Simulations*.  
Cambridge Univ. Press, Cambridge  
Adachi, I., Hayashi, C., & Nakazawa, K. 1976, *Prog. Theor. Phys.*, 56, 1756  
Agnor, C., Asphaug E. 2004, *ApJ*, 613, L157  
Agnor, C. B., Lin, D. N. C. 2012, *ApJ*, 745, 143  
Artymowicz, P. 1993, *ApJ*, 419, 166  
Bottke, W. F., Durda, D. D., Nesvorný, D., Jedicke, R., Morbidelli, A., Vokrouhlický, D., Levison, H. 2005, *Icarus*, 175, 111  
Brauer, F., Henning, T., & Dullemond, C. P. 2008, *A&A*, 487, L1  
Bryden, G., Chen, X., Lin, D. N. C., Nelson, R. P., Papaloizou J. C. B. 1999, *ApJ*, 514, 344  
Bryden, G., Różyczka, M., Lin, D. N. C., Bodenheimer, R. 2000, *ApJ*, 540, 1091  
Chambers, J.E. 2001, *Icarus* 152, 205  
Chambers, J. 2008, *Icarus*, 198, 256  
Ciesla, F. J., Hood, L. L. 2002, *Icarus*, 158, 281  
Connolly, H. C., Jr., Love, S. G. 1998, *Sci*, 280, 62  
Currie, T. & Sicilia-Aguilar, A. 2011, *ApJ*, 732, 24  
Cuzzi, J. N., Dobrovolskis, A. R., Champney, J. M. 1993, *Icarus*, 106, 102  
Cuzzi, J. N., Hogan, R. C., Shariff, K. 2008, *ApJ*, 687, 1432  
DeMeo, F. E., Carry, B. 2014, *Nature*, 505, 629  
Descamps, P., and Marchis, F. 2008, *Icarus*, 193, 74  
Desch, S. J., Connolly, H. C., Jr. 2002, *Meteoritics and Planetary Science*, 37, 183  
Dobbs-Dixon, I., Li, S.-L. & Lin, D. N. C. 2007, *ApJ*, 660, 791  
Dohnanyi, J. S. 1969, *JGR*, 74, 2531  
Fernandez, W.-H., Ip, J.A. 1984, *Icarus* 58, 109  
Garaud, P., Lin, D. N. C. 2004, *ApJ*, 608, 1050  
Garaud, P., & Lin, D. N. C. 2007, *ApJ*, 654, 606  
Goldreich, P., Ward, W. R., 1973, *ApJ*, 183, 1051  
Goldreich, P., & Tremaine, S. 1980, *ApJ*, 241, 425  
Gomes, R., Levison, H.F., Tsiganis, K., Morbidelli, A. 2005, *Nature* 435, 466  
Haisch, K. E., Jr., Lada, E. A., Lada, C. J. 2001, *ApJ*, 553, 153  
Hansen, B. M. S. 2009, *ApJ*, 703, 1131  
Hartmann, L. 1998, *Accretion Processes in Star Formation*.  
Cambridge Univ. Press, Cambridge  
Hayashi, C. 1981, *Progress of Theoretical Physics Supplement* 70, 35-53  
Heppenheimer, T. A. 1980, *Icarus*, 41, 76  
Ida, S., & Lin, D. N. C. 1996, *AJ*, 112, 1239  
Ida, S., Bryden, G., Lin, D. N. C., Tanaka, H. 2000, *ApJ*, 534, 428  
Ida, S. & Lin, D. N. C. 2004, *ApJ*, 604, 388  
Ida, S., Lin, D. N. C., & Nagasawa, M. 2013, *ApJ*, 775, 42  
Johansen, A., Oishi, J. S., Low, M.-M. M., Klahr, H., Henning, T., Youdin, A. 2007, *Nature*, 448, 1022  
Kelley, M. S., Gaffey, M. J. 2000, *Icarus*, 144, 27  
Kretke, K. A. & Lin, D. N. C. 2007, *ApJ*, 664, L55  
Kleine, T., Touboul, M., Bourdon, B., et al. 2009, *Geochim. Cosmochim. Acta*, 73, 5150  
Knezevic, Z., Milani, A. 2003, *Astron. Astrophys.* 403, 1165  
Kokubo, E., Ida, S., 1998, *Icarus*, 131, 171  
Lecar, M. & Franklin, F. 1997, *Icarus*, 129, 134  
Lee, M. & Peale, S. J. 2002, *ApJ*, 567, 596  
Lemaitre, A. & Dubru, P. 1991, *CeMDA*, 52, 57  
Leinhardt, Z. M., Stewart, S. T. 2012, *ApJ*, 745, 79  
Li, S. L., Agnor, C. B., & Lin, D. N. C. 2010, *ApJ*, 720, 1161  
Lin, D. N. C. & Papaloizou, J. 1986, *ApJ*, 309, 846  
Malhotra, R., Fox, K., Murray, C. D., & Nicholson, P. D. 1989, *A&A*, 221, 348  
Malhotra, R. 1993, *Nature* 365, 819  
Margot, J. L., Nolan, M. C., Benner, L. A. M., et al. 2002, *Sci*, 296, 1445  
Marchis, F., Hestroffer, D., Descamps, P. et al., 2006, *Nature*, 439, 565  
McSween, Harry Y. (1999). *Meteorites and their parent planets*.  
Cambridge Univ. Press, Cambridge  
Morbidelli, A., Levison, H.F., Tsiganis, K., Gomes, R. 2005, *Nature* 435, 462  
Morbidelli, A., Bottke, W., Nesvorný, D., Levison, H. F. 2009, *Icarus*, 204, 558  
Murray, C. D., Dermott, D. F. 1999, *Solar system Dynamics*.  
Cambridge Univ. Press, Cambridge  
Nagasawa, M., & Ida, S. 2000, *AJ*, 120, 3311  
Nagasawa, M., Tanaka, H., Ida, S. 2000, *AJ*, 119, 1480  
Nagasawa, M., Ida, S., Tanaka, H. 2001, *EP&S*, 53, 1085  
Nagasawa, M., Ida, S., Tanaka, H. 2002, *Icarus*, 159, 322  
Nagasawa, M., Lin D., Thommes, E. 2005, *ApJ*, 635, 578  
Nesvorný, D., Vokrouhlický, D., Bottke, W. F. 2006, *Sci*, 312, 1490  
O'Brien, D. P., Morbidelli, A., Bottke, W. F. 2007, *Icarus*, 191, 434  
Paardekooper, S. J., Baruteau, C., Kley W. 2011, *MNRAS*, 410, 293  
Palmer, P. L., Lin, D. N. C., & Aarseth, S. J. 1993, *ApJ*, 403, 336  
Petit, J., Morbidelli, A., Chambers, J. 2001, *Icarus* 153, 338  
Pollack, J. B., Hubickyj, O., Bodenheimer, P., Lissauer, J. J., Podolak, M., & Greenzweig, Y. 1996, *Icarus*, 124, 62  
Safronov, V.S. (1969), *Evolution of the Protoplanetary Cloud and Formation of the Earth and Planets*, Nauka, Moscow.  
NASA TTF-677  
Stewart, S. T., Leinhardt, Z. M. 2012, *ApJ*, 751, 32  
Su, K. Y. L., Rieke, G. H., Malhotra, R., et al. 2013, *ApJ*, 763, 118  
Supulver, KD, Lin D. N. C. 2000, *Icarus*, 146, 525  
Thommes, E., Nagasawa, M., & Lin, D. N. C. 2008, *ApJ*, 676, 728  
Tsiganis, K., Gomes, R., Morbidelli, A., Levison, H.F. 2005, *Nature* 435, 459

- Walsh, K. J., Morbidelli, A., Raymond, S. N., O'Brien, D. P.,  
Mandell, A. M. 2011, *Sci*, 475, 206
- Ward, W. R. 1981, *Icarus*, 47, 234
- Ward, W. R. 1989, *ApJ*, 345, L99
- Ward, W. R. 1993, *Icarus*, 106, 274
- Ward, W. R. 1997, *Icarus*, 126, 261
- Weidenschilling, S. J. 1977, *MNRAS*, 180, 57
- Weidenschilling S. J., Cuzzi J. N., 1993, in Levy E. H., Lunine J.  
I., eds, *Protostars and Planets III Formation of planetesimals  
in the solar nebula. Protostars and Planets III*, University of  
Arizona Press, p.1031-1060
- Weidenschilling, S. J., Spaute, D., Davis, D. R., Marzari, F.,  
Ohtsuki, K. 1997, *Icarus*, 128, 429
- Wetherill, G. W. 1980, *ARA&A*, 18, 77
- Wetherill, George W., " Origin of the asteroid belt" *Asteroids II*;  
*Proceedings of the Conference*, Tucson, AZ, Mar. 8-11, 1988  
(A90-27001 10-91). Tucson, AZ, University of Arizona Press,  
1989, p. 661-680
- Wetherill, G.W., Stewart, G.R. 1989, *Icarus* 77, 330
- Wetherill, G.W. 1992, *Icarus* 100, 307
- Whipple, F. L. 1972, in *From Plasma to Planet*, ed. A. Elvius  
(New York: Wiley), 211
- Youdin, A. N., Shu, F. H. 2002, *ApJ*, 580, 494
- Youdin, A., Goodman, J. 2005, *ApJ*, 620, 459
- Zappalà, V.; Cellino, A.; dell'Oro, A.; Paolicchi, P., "Physical  
and Dynamical Properties of Asteroid Families" in *Asteroids  
III*, W. F. Bottke Jr., A. Cellino, P. Paolicchi, and R. P. Binzel  
(eds), University of Arizona Press, Tucson, p.619-631
- Zhou, J. L., Lin, D. N. C., & Sun, Y. S. 2007, *ApJ*, 666, 423
- Zuckerman, B., Forveille, F., Kastner, J. H. 1995, *Nature*, 373,  
494